• U C •

FCTUC FACULDADE DE CIÊNCIAS
E TECNOLOGIA
UNIVERSIDADE DE COIMBRA

DEPARTAMENTO DE FÍSICA

Mestrado Integrado em Engenharia Biomédica

Deposition of AlN_x thin films on polymers for the development of biosensors

Miguel Rodrigues

Coimbra, Setembro 2013

FCTUC FACULDADE DE CIÊNCIAS
E TECNOLOGIA
UNIVERSIDADE DE COIMBRA

DEPARTAMENTO DE FÍSICA

Mestrado Integrado em Engenharia Biomédica

Deposition of AlN_x thin films on polymers for the development of biosensors

Dissertação submetida à Faculdade de Ciências e Tecnologia da Universidade de Coimbra para obtenção do grau de Mestre em Engenharia Biomédica sob a orientação do Professor Carlos Fonseca e do Professor Doutor Albano Cavaleiro

Com a colaboração institucional de:

Universidade do Porto
Faculdade de Engenharia
FEUP

Miguel Rodrigues

Coimbra, Setembro 2013

Júri

Presidente:
Nome: António Adriano Castanhola Batista
Categoria: Professor Auxiliar
Departamento: Departamento de Física

ORIENTADORES:

Nome: José Carlos Magalhães Duque da Fonseca
Categoria: Professor Auxiliar
Instituição: Departamento de Engª Materiais da Universidade do Porto

Nome: Albano Augusto Cavaleiro Rodrigues de Carvalho
Categoria: Professor Catedrático
Departamento: Departamento de Engenharia Mecânica

VOGAIS:

Nome: Manuel Evaristo
Categoria: Investigador Pos-Doc
Instituição: Departamento de Engenharia Mecânica

Nome: José Filipe Vilela Vaz
Categoria: Professor Associado
Departamento: Departamento de Física da Universidade do Minho

To Artur and Sãozinha

Agradecimentos

Em primeiro lugar gostaria de agradecer às pessoas que directamente contribuíram para a concretização deste trabalho:

Aos meus orientadores, Prof. Doutor Albano Cavaleiro e Prof. Doutor Carlos Fonseca, por me terem dado a possibilidade de pertencer a um grupo de investigação como o SEG-SEMUC, pela orientação dada, pelas críticas, sugestões ou esclarecimentos que tanto me foram úteis, e pelo tempo e recursos disponibilizados no meu projecto.

Ao Dr. Manuel Evaristo, por toda a ajuda que me deu no desenrolar da parte experimental deste projecto, por toda a paciência que teve em explicar-me os processos físicos inerentes à pulverização catódica; mas também por ter tido a disponibilidade em me mostrar outros equipamentos do laboratório e de como funciona o mundo da investigação.

Ao Dr. João Carlos Oliveira e à Dra. Ana Paula Piedade que, apesar de não estarem directamente ligados ao meu projecto, tiveram uma grande disponibilidade para discutir comigo muitos dos resultados obtidos ao longo da parte experimental deste trabalho.

Ao Ricardo Serra e ao Filipe Fernandes pela ajuda com as técnicas de caracterização. Ao Fábio Ribeiro por todo o apoio que me deu desde o meu primeiro contacto com o grupo.

Por fim, a todos os elementos do laboratório de materiais do Dep. de Eng. Mecânica da UC, (às colegas de sala em especial) pela simpatia e disponibilidade para ajudar no que fosse preciso.

Um agradecimento aos elementos da Universidade do Minho (em especial ao Joel Borges) pela ajuda que me deram com as medições de resistividades.

Ao meu pai, pela preciosa ajuda com a preparação das amostras para os exames SEM.

À Ana Farinha, ao Sandro Norim e ao Fernando Couto pois sem eles a redacção desta tese não teria sido possível.

Agora, resta agradecer às pessoas que não tiverem directamente ligadas ao projecto:

A toda a gente que me proporcionou boa companhia e boa amizade em alguma fase do curso, e que pelas vicissitudes da vida já não temos grande contacto ou amizade, não esquecerei do quanto foram importantes.

Aos ilustres residentes do número 4 da Rua da Alegria e do número 44 da Rua da Matemática, pelas nossas calorosas discussões acerca do tema mais sério ou mais fútil do

momento, mas mais importante por todos os bons e maus momentos que atravessamos juntos. Muito do que sou devo-o a vocês.

A todos os meus amigos, em especial ao Romão Suave por me ter ensinado que a vida é demasiado importante para ser levada a sério.

Por ultimo, e porque o melhor fica sempre para o fim:

À Anita; obrigado por me fazeres sentir a pessoa mais feliz do mundo. Espero que o futuro nos reserve muitos projectos musicais (entre outros) em conjunto!!

Finalmente à minha querida família: aos meus irmãos, pelo tanto que se preocupam comigo; e uma forma muito muito especial aos meus pais a quem, orgulhosamente, dedico este trabalho.

Muito obrigado por todos os sacrifícios que fizeram para que nós pudemos vir para a universidade, obrigado por me terem ensinado o valor do trabalho e por terem estado sempre sempre presentes! Obrigado meus velhinhos preferidos!!

Resumo

A medição de biossinais assume actualmente uma importância elevada, uma vez que pelos dados obtidos é possível aceder a uma vasta gama de informações do nosso corpo, que são muito úteis na ajuda aos clínicos para melhorar a saúde dos pacientes. Nos instrumentos de medição, os eléctrodos assumem uma importância extrema já que representam a interface corpo-instrumento de medição, e da sua correcta actuação depende a obtenção de um sinal com boa qualidade. Todos os eléctrodos actualmente utilizados compreendem limitações, relacionadas ou com a sua aplicação (eléctrodos húmidos) ou com problemas de ruído (eléctrodos secos).

O objectivo desta tese é investigar um protótipo de eléctrodo com um princípio de funcionamento diferente dos eléctrodos actuais. O eléctrodo pretendido baseia o seu funcionamento na aplicação de pulsos de corrente, que por efeito Joule aplicam um aquecimento localizado da pele permitindo a formação de microporos na camada externa da pele, o *stratum cornenum*, responsável pelas propriedades de barreira da pele. A formação destes microporos possibilita uma melhor obtenção dos iões responsáveis pelos bio sinais, eliminando, portanto, os problemas associados aos eléctrodos actuais (todos causados pela barreira da pele ao fluxo destes iões).

Para este fim, procedeu-se à deposição de filme substequiométrico de nitreto de alumínio resistivo sobre um substrato polimérico (usando a pulverização catódica como técnica de deposição). As características do filme foram optimizadas para se obter espessuras e resistividades desejadas, 200-300 nm e 0,001-0,1 ohm.cm, respectivamente. Estas características foram primeiramente aproximadas usando silício e vidro como substratos. Depois, filmes com estas características foram depositados em polímeros. Poliuretano foi inicialmente escolhido como substrato, no entanto apresentou uma deformação sobre calor levando à fissuração do filme. Pelo contrário, usando policarbonato como substrato, os filmes revelaram boa integridade.

Para o revestimento do policarbonato, a deposição dos filmes foi estudada mais em detalhe. Condições de etching foram optimizadas, com a definição de dois tempos de tratamento apropriados para a deposição dos filmes, com estes a apresentarem muito boa adesão e resistividades eléctricas dentro da gama pretendida, servindo o objectivo do projecto.

Abstract

Nowadays, biosignals recording is extremely important since from the obtained data it is possible to access a wide range of important body informations, which are highly useful to help clinicians to improve patient's health. Within measuring devices, an electrode assumes an extreme importance since it represents the body-measuring instrument interface, and its proper functioning is essential to obtain a good signal. All the currently available electrodes comprise limitations related either to their application (wet electrodes) or noise problems (dry electrodes).

This thesis goal is to investigate an electrode prototype with a different working principle from the current ones. The intended electrode relies on the application of pulses of current, which by Joule effect provide a localized heating on the outer layer of skin, stratum corneum, responsible by the barrier properties of skin. This heating has as consequence the formation of micropores in this layer which increase its permeability. Thus, the outward flow of the ions responsible for the biosignais becomes easier and the problems associated with the currently used electrodes (all caused by skin's barrier to flow) are eliminated.

For this purpose, a resistive aluminum nitride sub stoichiometric film was intended to be deposited onto a polymeric substrate (using sputtering as deposition technique). Film characteristics were optimized in order to obtain the desired thickness and resistivity, 200-300nm and 0,001-0,1 ohm.cm, respectively. These features were firstly pursued using silicon and glass as substrates. Subsequently, films with these characteristics were deposited onto polymers. Firstly polyurethane was chosen as substrate however it underwent deformation under head leading to cracks on the films' structure. In contrast, when using polycarbonate as substrate, films revealed good integrity.

For the polycarbonate coating, films deposition was further studied. Eching conditions were optimized, with the defining of two etching treatments suitable for the films deposition, with films revealing a very good adhesion and an electrical resistivity within the desired range were obtained, serving the purpose of the project.

Table of contents

Figure Index

Table Index

Abbreviations

AFM: atomic force microscopy

Ag: silver

AgCl: silver chloride

AlN: aluminum nitride

Ar^+: argon ions

CA: contact angle

Cl^-: chloride ions

ECG: Electrocardiogram

EDS: energy dispersive X-ray spectroscopy

EEG: Electroencephalogram

Ep: ionization probability

IBS: ion beam sources

K^+: potassium ions

N_2: nitrogen

Na^+: sodium ion

PC: polycarbonate

PU: polyurethane

PVD: phisical vapour deposition

Ra: average roughness

SC: *stratum corneum*

SEM: scanning electron microscope

Vmin: minimum target potential to sustain the discharge

XRD: X-ray difraction

Chapter 1
Introduction

1.1 Bioelectric signals

Several biologic systems comprise electric activity, which can take the form of a constant dc electric field, current or charge-carrying particles flow or a time-dependent electric field or current, related with some biochemical or biological phenomenon [1]. Bioelectric signals are usually defined as low amplitude and relatively low frequency electrical signals [2] associated with the changes in the distribution of ions or charged molecules that occur in a biologic structure as a result of biochemical reactions or a phenomenon related with a local anatomy alteration [1]. In the medical field, several signals can be considered, depending on their origin. Biosignals can be divided in: electric, magnetic, and acustic, among others [2, 3].

Biopotential recordings (table 1.1) are extremely important either for clinical or research applications, providing a wide range of information, which after processing is useful for medical monitoring and treatment, thus improving patient's health [4]. Electrocardiogram (ECG) and Electroencephalogram (EEG) are the biopotential recordings most commonly assessed in medical applications [3].

Table 1.1 – Bioelectrical signals and their sources. Adapted from [1]

Bioelectric Signal	Abbreviation	Biologic Source
Electrocardiogram	ECG	Heart (body surface)
Cardiac electrogram	-	Heart (within)
Electromyogram	EMG	Muscle
Electroencephalogram	EEG	Brain
Electrooptigram	EOG	Eye dipole field
Electroretinogram	ERG	Eye retina
Electrogastrogram	EGG	Stomach
Galvanic skin reflex	GSR	Skin

1.1.1 Action potential: the origin of the bio-electric signal

Due to a complex self regulatory system, nerve and muscle cells generate bioelectric signals when their membrane potential generates an action potential [2]. In the case of a single cell measurement, where specific microelectrodes as micro needles are used as sensors, this action potential (fig. 1.1) is itself the electrical signal [3]. Concerning a surface electrode measurement, the electric activity generated by a single cell is too small to be measured, thus; in this case, a measurement corresponds to a sum of millions of signals which represent a time and spatial synchrony action potential activity [5].

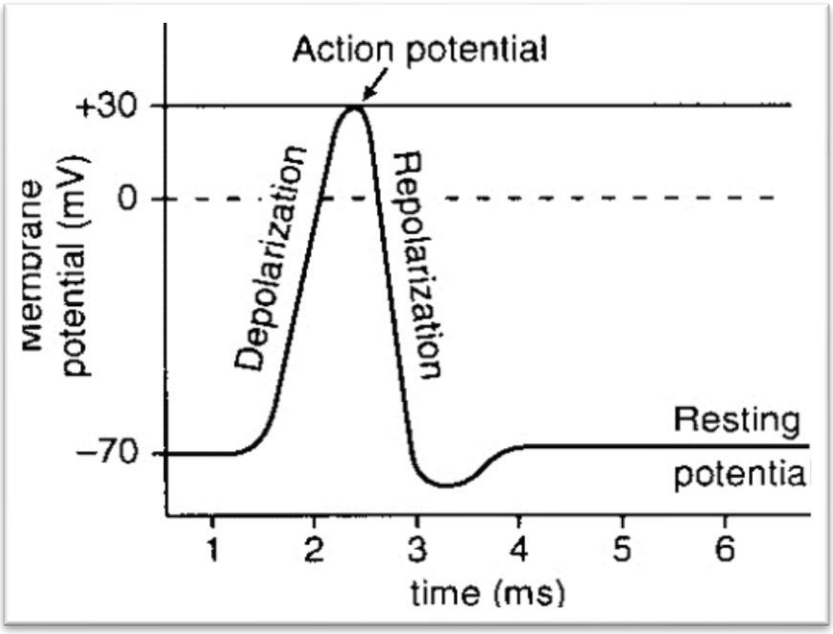

Fig. 1.1 – Nerve cell action potential [6]

An action potential corresponds to a quickly (in the millisecond range) reversal of the electric polarization of the membrane of a nerve or muscle cell [7] as a response to a stimuli; it is responsible for the neuronal signal propagation on nerve cells [5] and for the necessary contractions for movement on the muscle cells [7].

In the resting state, a neuron or muscle cell has a negative electric polarization which means that the interior of its membrane has a negative charge when compared with the exterior fluid. This is a consequence of the high concentration of (positive) sodium ions (Na^+) in the outside and the high concentration of (negative) chloride ions (Cl^-) combined with a lower concentration of (positive) potassium ions (K^+) in the interior [7]. This is known as the resting potential and for a nerve cell it is around -90mV [5].

If the cell is stimulated by the action of neurotransmitters or protein-receptors, the cell's membrane becomes permeable to Na^+ by the opening of channel –shaped protein molecules in the membrane, and the potential becomes less negative [5, 7]. If this potential reaches a critical state, known as threshold potential, these channels open completely allowing the passage of a high quantity of Na^+ ions by passive diffusion, due to the concentration gradient, to the interior of cell [5]. This initiates the depolarization, which ends with the peak of the action potential characterized by a positively charged interior and a negative charged exterior [5, 7]. Depolarization activates sodium entrance channels on the vicinity so that the impulse is propagated through the fiber [7].

The repolarization phase begins with the closing of Na^+ channels, and the opening of K^+ channels, which allows the passage of K^+ for the exterior of the membrane allowing the action potential to decline from its peak [7]. Finally, the membrane permeability to K^+ returns to normal with its potential coming back to the resting state potential, and the cell is ready for a new action potential [5].

1.1.2 Electrocardiogram (ECG)

An ECG measures electrical variation of the ionic potential of the heart [2]. The heart is composed by pacemaker, electrical conducting and myocardial cells which, by means of action potentials, produce a wave of depolarization that is transmitted across the heart, resulting in the flow of ionic current [8]. The common ECG is the surface detection of the electrical activity of myocardium cells [9], which represent the majority of cardiac cells and reflect the heart's contractile machinery [8].

Since the body is a volume conductor and an alteration on heart's potential is transmitted throughout the body [8], ECG is measured by small variations of potential on skin's surface [8].

The standard exam consists merely in a non-invasive placement of three electrodes in different points of the body [9]. An abnormal heart's activity can reflect problems as myocardial infarction or different cardiac arrhythmias, among others [8], rendering ECG a very important and widely used exam in medical field. A typical ECG waveform is shown in fig 1.2.

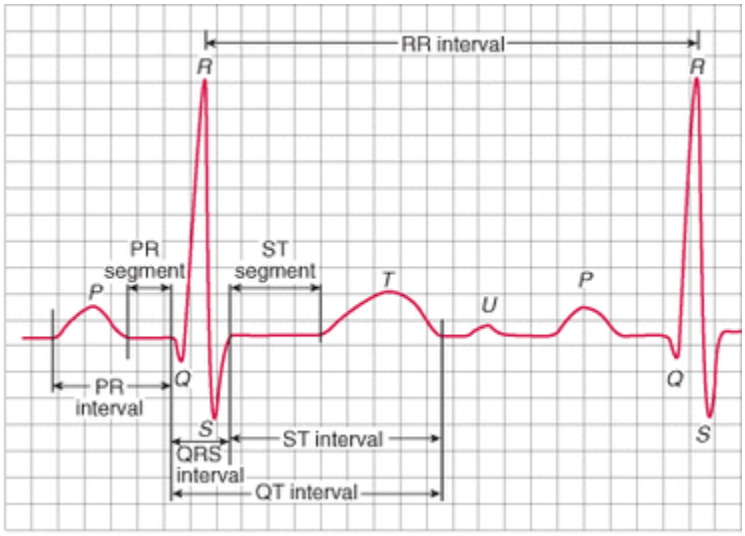

Fig. 1.2 – Typical ECG tracing of the cardiac cycle. [10].

From fig 1.2 it is possible to notice the different waves of the ECG signal. It consists of a P wave (atrial depolarisation), a QRS complex (it produces Q, R and S waves and represents rapid ventricular depolarization), a T wave (ventricular repolarisation) and a U wave (repolarisation of the purkinje fibers, the electric conducting cells; normally invisible) [10].

1.1.3 Electroencephalogram (EEG)

An EEG consists on the recording of electrical activity along the human scalp as a result of ionic current flows generated by neurons [2, 8]. Normally, an EEG waveform has amplitudes between 10 and 100 μV [4].

The brain is composed by two types of cells: neurons and glia cells [2, 8]. Neurons, due to action potentials mechanisms, are responsible for the charges transportation across the membranes of the brain [2]. Synapses are communication mechanisms between neurons. The pre-synaptic neuron, due to an action potential, causes the release of neurotransmitters into the synaptic cleft; posteriorly neurotransmitters bind to the post-synaptic neurons. The action of many of these neurotransmitters causes, in the extracellular space, current variations which are responsible for the EEG potentials generation [8].

Fig. 1.3 shows the EEG signal for different neuronal waves, dependent on the conscientious stage. EEG is a powerful non invasive tool for the monitoring of brain's functionality, since an anomaly in the EEG data allows clinicians to detect several brain disorders as epilepsy, sleep disorders or strokes, among others [8].

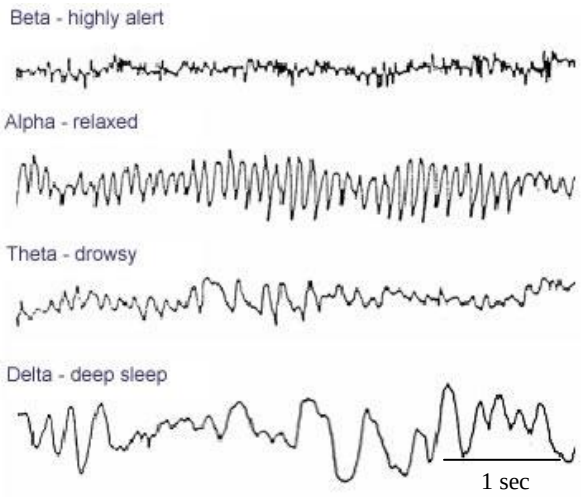

Fig. 1.3 – Typical EEG waves: their frequency and amplitude vary according to the conscientious stage. Adapted from [11].

1.2 Biopotential Electrodes/Recording Electrodes

Ionic current responsible for the bioelectric signals flows within the human body, being possible to sensor it using an electrode. A common electrode used to measure bioelectrical information corresponds to an electrical transducer which, in contact with the tissue surface, converts the ionic current to electronic one [4], allowing the flow of the electric current to the measuring instrument where it is analyzed, interpreted and converted to a readable form [9].

The electrode is the critical component of the monitoring set-up since it works as an interface between the body and the electronic device [5], which makes it crucial for the important current conversion, referred above.

Bio electrodes can be divided into two major categories: invasive and non invasive [5].

1.2.1 Invasive electrodes

Invasive electrodes (Fig. 1.4) are micro needles surgery implanted on sub-cutaneous tissues [5] providing an excellent signal quality with minor noise problems. However, due to the need for the surgery for its implantation, these electrodes comprise the risk of infections on the patient [12].

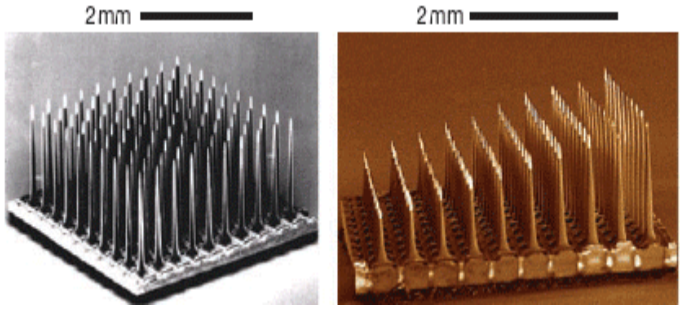

Fig. 1.4 – Invasive electrodes. Adapted from [13].

1.2.2 Non invasive electrodes

In the case of a non invasive measurement, wet and dry electrodes (which are placed over skin surface) can be considered [14]. As opposed to invasive recording, non invasive electrodes have to deal with skin barrier drawback, and with its major inherent problem: the attenuation of signal amplitude [5].

1.2.2.1 Wet electrodes

"Wet electrodes" (Fig.1.5), namely the silver/silver chloride (Ag/AgCl) electrodes, are the main electrodes used in clinical field [9, 15, 16]. They require the use of an electrolytic gel between the skin and the electrode surface [17, 15, 16, 4], which makes the outer skin layer more ion conductive, reducing its impedance [8].

Fig. 1.5 – Wet electrodes [18]

Oxidation and reduction reactions (equation 1) occur in the skin-electrode interface [4], allowing the ion-electron exchange [5].

$$AgCl + e^{-} \text{------>} Ag^{0} + Cl^{-} \quad \text{(Equation 1)}$$

In the case of EEG recordings, the use of a wet electrode comprises skin abrasion [17, 14] in order to obtain a lower contact interface impedance (5 – 10 KΩ). This will allow the electrolytic gel to be buffered into the outer and inner layers of epidermis, and it will thus enable the achievement of a good and stable quality signal [4].

The need for the use of an electrolytic gel renders these electrodes disadvantageous since its application is long time consuming [4, 16], it may promote skin irritation on some patients [14] or eventually dry out [4, 16]. Gel dehydration may constitute a serious problem since signal quality may be compromised over time, due to problems related with noise and other artifacts [17] derived from the increase of electrode impedance [4], rendering these electrodes not suitable for long time applications.

1.2.2.2 Dry electrodes

The above referred limitations led to the development of different electrodes, the so-called "dry electrodes" [16].

Dry electrodes do not require either the use of an electrolytic gel between the skin electrode interface or the skin/scalp preparation [15, 19]; dry electrodes thus outperform wet electrodes in the reduced set-up times and subject discomfort as well as in gel level maintenance dispense [20].

These electrodes can be constructed from metals or flexible metal coated polymers [17] and can be divided in two major groups: passive and active electrodes [4].

Passive electrodes consist on a sensor connected to an ultra-high input impedance biosignal amplifier [4, 16] through a carefully shielded wire [19].

Their signal quality is deeply dependent on the pressure applied to the electrode, which is crucial to obtain lower skin-electrode impedances [12], condition required for a good signal quality without noise artifacts [21]. Despite of the inherent source of artifact provided by a pressure that is not easily controlled, it may also be unpleasant for the patient [12].

Active dry electrodes make use of pre amplification circuits (with gains of 1-10x) inside the electrode overcoming the passive electrodes problems, thus working for higher skin – electrode impedances; which, as opposed to passive electrodes, may be above 10 KOhm [21].

However, the use of active electronics in the electrode renders it bulkier and more expensive [16], which has led to their commercial rejection [4, 15].

Fig. 1.6 – Active dry electrodes [22].

Regarding biopotential non invasive recordings; both the wet and the dry electrodes present limitations. While wet Ag/AgCl electrodes have their reliability, and good signal quality well established [5], they are disadvantageous concerning the need for the use of electrolytic gels and the consequent limitations [4, 16]. On other hand, dry electrodes offer the possibility to exclude the use of electrolytic gels [15, 19], however its use comprises several limitations related with noise problems (passive electrodes) or its price (active electrodes) [21].

1.3 New Electrode Concept

1.3.1 AlN_x electrode

The disadvantages/problems of either the wet or the actual dry electrodes related with the signal attenuation inflicted by the skin are quite established [5]. The proposed electrode is intended to overcome the skin barrier drawback, exempting at the same time either the need for the use of electrolytic gels or active pre-amplificatory circuits.

In order to achieve the above referred features, this prototype electrode consists in a 200 – 300 nm thick resistive AlN_x track deposited onto a polymeric substrate (Fig. 1.7), rendering the electrode cheaper and potentially more flexible than the one composed only by a metal/ceramic substrate.

With the application of short current pulses onto these tracks, a localized and controlled skin heating is achieved by Joule effect, disrupting the *stratum corneum* layer, which heating effects are detailed explained below, and thus facilitating the passage of the electro physiologic signals out of the skin.

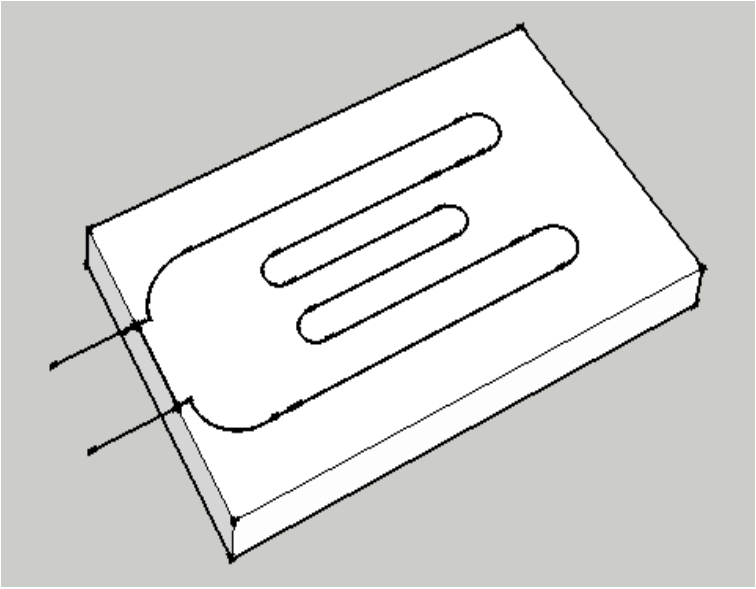

Fig. 1.7 – AlN_x electrode design.

1.3.2 Effects of heat on skin permeability

Stratum corneum (SC), the outer horny layer of skin, is an approximately 10-30 μm thick layer (except on the palms of hands and feet where it is ten times thicker) [23, 24] composed by 25-30 layers of flattened dead cells [25].

SC structure is a unique complex architecture which forms a compact moisture barrier much less permeable either for the entrance of molecules into the body or the outward of analytes from the inside of the body when compared with the gastric or oral mucosa [24].

This layer is composed by keratin-filled dead cells named corneocytes [24, 26], surrounded by crystalline lamellar epidermal lipids [24] which act as a cement, packing the corneocytes in a ordered state and thus playing an important role on this barrier function [27].

Microporation

Microporation designates the creation of a hole or micropore in a biological membrane as skin (*stratum corneum*) [28].

A microporator or porator is a device capable of creating micro-holes [24], which typically range from 1 to 1000 microns in diameter and should be deep enough to lessen barrier properties of SC without damaging the inner tissues [28].

Among the different techniques to perform microporation one can distinguish electrical methods: iontophoresis or electroporation [29], the use of micro needles [24] or the application of pulsed thermal energy [30]. Each method has its own micropore creation method [29]: electrical ones are related with the structural rearrangement of stratum corneum; micro needles rely on the puncturing of the SC; and the use of thermal energy consists on the decomposition and removal of a small area of stratum corneum in order to create a micron-scale hole [24].

When a heat source gets in contact with a small area of the skin and provides sub second intervals of heat, thermal energy is transmitted through the SC within this small

area, causing the vaporization of the tissue-bound water content and other vaporizable substances in the vicinity of the application site [30], thereby causing a removal of cells [24, 30] in the outer layers of the SC.

As subsequent pulses are applied the same effects are achieved on the additional layers of stratum corneum, leading to a "vertical" microhole formation (fig. 1.8) which crosses the entire SC [30, 31].

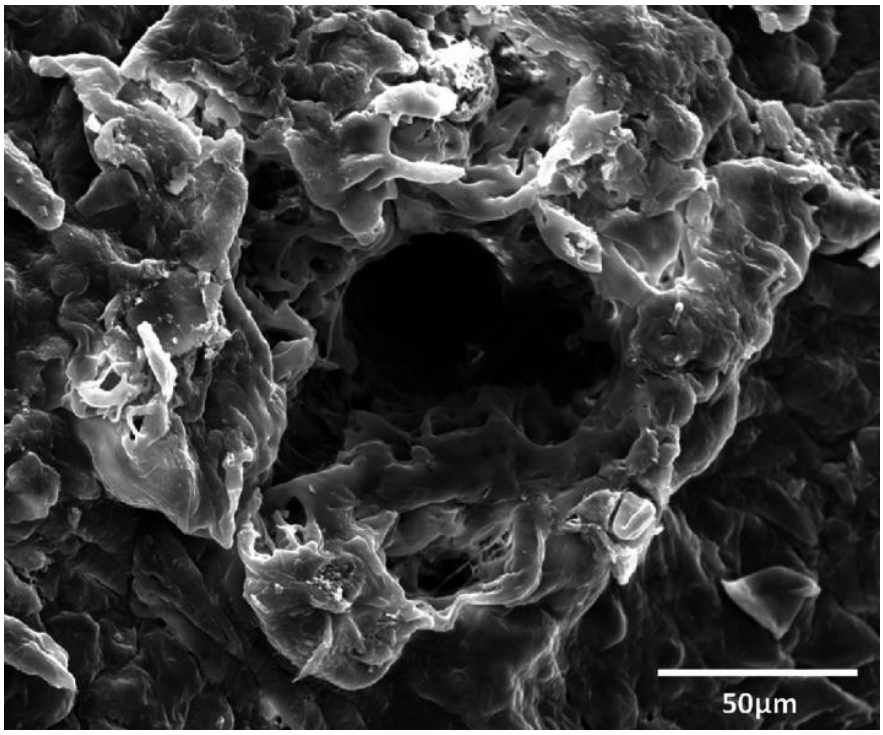

Fig. 1.8 – SEM picture of a single pore. Adapted [31].

With the control of the heat pulse duration, and a long enough interpulse spacing, the energy conducted into the viable layers of epidermis can be minimized leading to lower temperatures attained in this tissue so that the microporation process can occur without its damage and without any subject sensation of discomfort [30].

Since SC is chiefly responsible for the skin barrier to permeability [25, 27], by disrupting this barrier with skin exposure to heat, and consequent microporation, the permeability can be largely increased [30, 27, 29].

A Sputter Deposited Thin Film Tissue Interface (TFTI) Device is one of the several already proposed examples by Altea therapeutics to perform microporation and basically relies on the deposition of resistive element pattern traces, as tantalum, on a suitable substrate, as polyamide [24] combined with a transdermal delivery device composed by a drug source and a dermal contact layer allowing the drug source to be permanently in contact with skin [28].

This device, after heating the skin, allows the enhancement of transdermal flux of drugs, enzymes or other agents [28]. Fig 1.9 shows the improvement of the transport of calcein across the human epidermis with a localized heat application.

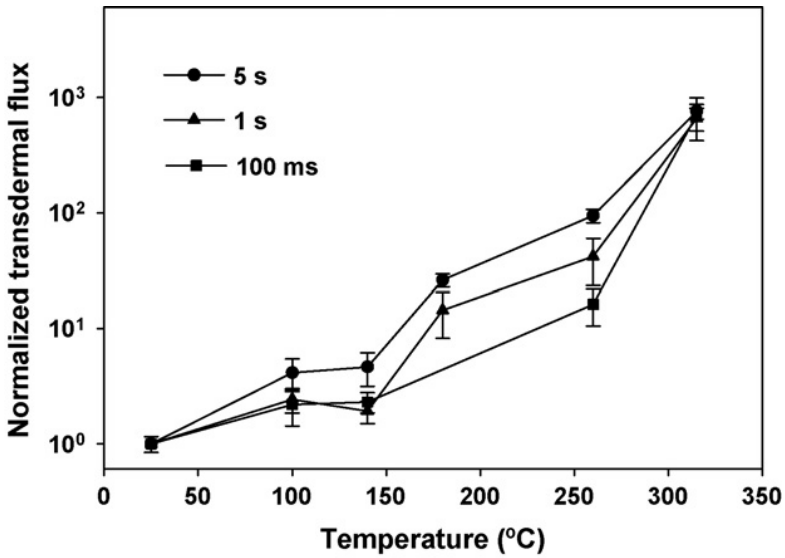

Fig. 1.9 – Effect of temperature and heating time on the flux of calcein across human epidermis. [27].

From fig. 1.9, one can notice that transdermal flux is dependent on the temperature, but also on the time of exposure; in fact, skin permeability is much more dependent on temperature that on the time of exposure [27]. Moreover, depending on its temperature and duration, skin heating effects are reversed after exposure, returning skin's permeability to normal [32].

1.3.3 Aluminium nitride

Aluminium nitride is a ceramic compound, with a high melting point (above 2500 ºC) [33], which commonly crystallizes in a wurztite-like hexagonal lattice structure, with a large bandgap (~6.2 eV) [34].

AlN is known for its good chemical, thermal and mechanical stability [34], being an excellent thermal conductor with a resistivity of 10^{12} Ohm.cm [35]. Considering a sub stoichiometric AlN thin film (AlN_x), its resistivity can largely decrease when compared to the AlN bulk material. Indeed, for $0,5 < x < 0,8$ resistivities from 10^{-3} to 10^{3} ohm.cm can be observed [33]

Due to its properties has been widely used in the manufacturation of high power and high temperature electronic devices, among others [35]. Table 1.2 summarizes some AlN characteristics.

Table 1.2 – Typical values for some of the AlN major properties. Adapted from [33]

Property	Typical values
Density ($g.cm^{-3}$)	3,26 - 3,32
Toxicity	None
Melting temperature (K)	2800 - 3273
Hardness (Gpa)	11 - 12,3
Coefficient of thermal expansion 20-400ºC ($x10^{-6}K^{-1}$)	4,5 - 5,7
Thermal conductivity (W/m.K)	140 - 180
Electrical resistivity (ohm.cm)	$> 10^{14}$

Chapter 2
Experimental details

2.1 Theory of deposition process

2.1.1 Sputter Etching: Kauffman Ion source

Sputter etching (surface activation) is the phenomena in which atoms are removed from a surface due to the effect of irradiation of energetic ions [36]. It is applied on the material that is intended to serve as substrate for the posterior film deposition.

An ion source can be defined as a plasma source coupled with an ion extraction system [37]. The first represents the discharge plasma region while the last one represents the grid system [38].

The etching system used in this study is a hot cathode ion source, also known as a Kaufman Ion Source (fig 2.1), this kind of source makes part of the Ion Beam Sources (IBS) family [39], and is widely used in sputter etching [36, 39].

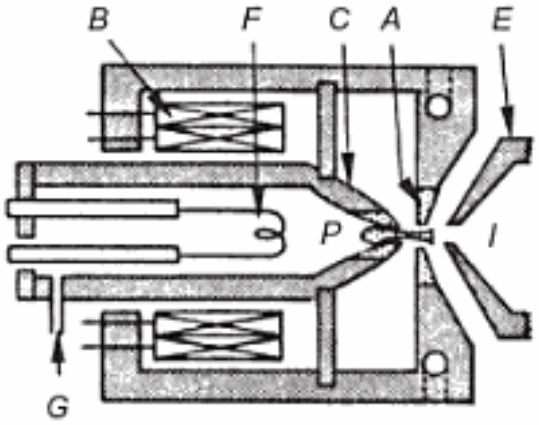

A – Anode
B – Magnetic field
C – Cathode
E – Accelerating Electrode
F – Tungsten Filament
G – Gas Inlet
P – Plasma
I – Window

Fig 2.1 – Representation of a hot cathode ion gun. Adapted from [36].

In a Kaufman Ion Source the plasma is produced in a pre-chamber which is placed in a region away from the surface which is desired to treat [40].

The operation of this device is based on the emission of electrons by a thermionic tungsten hot filament, necessary to sustain a magnetically confined plasma discharge obtained due to the application of a discharge voltage between the hot filament F and the anode A (fig 2.1) [38, 39]. The emitted electrons suffer the effect of a magnetic field, which is used to control their motion, forcing them to take helical paths before being collected in the anode, thus increasing the number of collisions and ionization per electron [37].

The grid system confines the electrons to the plasma region and allows the extraction of the Ar^+ ions by the application of a specific potential between each grid [40]. During extraction, this high electrical field accelerates the ions giving them a kinetic energy dependent on the conditions applied to the grids [37].

2.1.2 Depositon Technique: Pulsed Magnetron Sputtering (PMS)

Magnetron Sputtering is a PVD(Phisical Vapour Deposition) in which atoms are detached from the target (cathode) as a result from the incidence of energetic ions generated in a glow discharge plasma situated in front of the target [40, 41].

Before the deposition process, the deposition chamber is pumped down to a low base pressure (fig 2.2 a). After that, an inert gas (usually Argon) is fed into the system. The process starts when an electric field is applied between the cathode (target) and the deposition chamber walls [36]. The inert gas, also known as working gas, is then ionized due to the action of the electric field, and its ions are accelerated towards the target removing specimens from its surface as a consequence from the momentum transfer (fig 2.2 b) [43, 44]. This bombarding also results in the removal of secondary electrons from target surface. These electrons are forced to travel near the target surface due to the effect of the association of the electric field with a magnetic field placed behind the target. This fact will further increase the ionization of the working gas giving rise to a higher atoms removal in the target. The removed atoms travel towards the substrate, being deposited onto it [42].

In reactive magnetron sputtering, one or more species to be deposited are fed in the system in the gaseous form [43]. In this method, the target is equally sputtered but by the

addiction of the reactive gas to the chamber, a reaction will occur between the ejected atoms and the reactive gas (fig 2.2 c), being the resulting compound deposited onto the substrate (fig 2.2 d). It is one of the most versatile sputtering techniques to deposit oxides and nitrides [45].

This technique has the advantage of allowing the deposition of an insulating material, starting from a metallic target, using a D. C. power supply. It is also possible to control the composition of the deposited films, by varying the reactive gas flow [44].

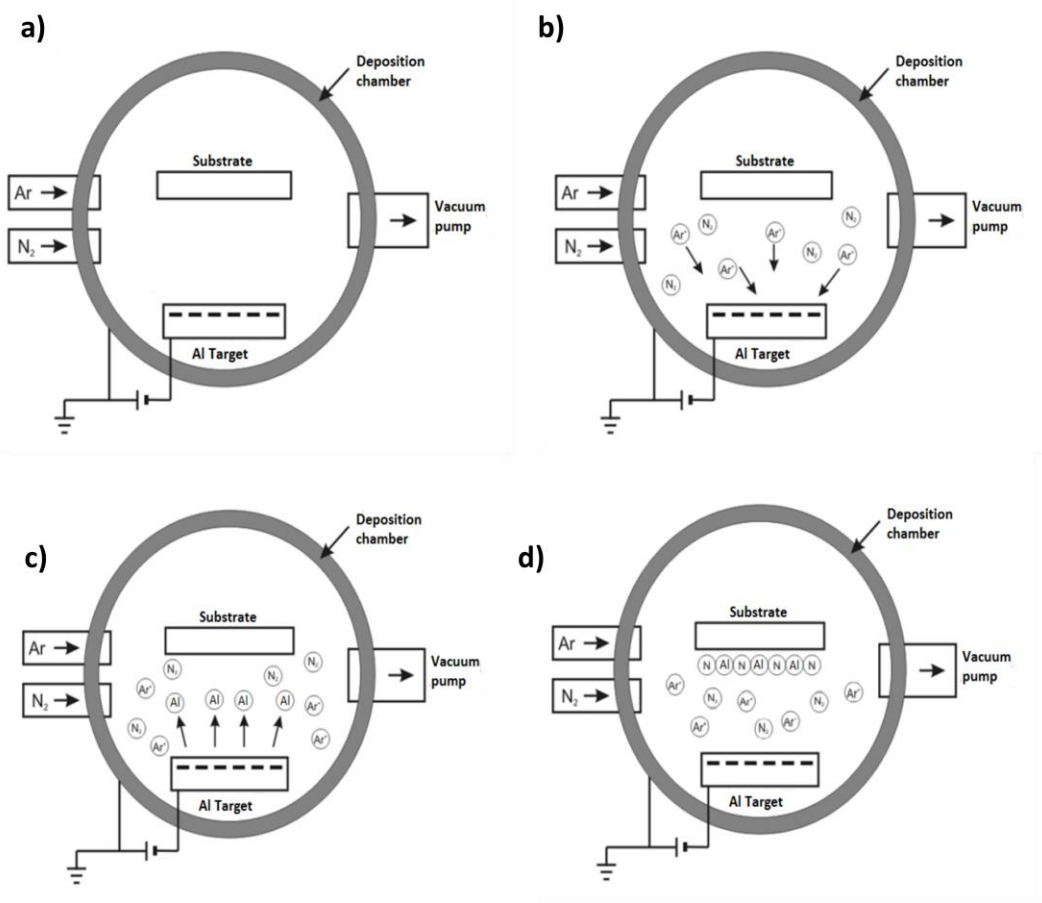

Fig 2.2 – Representative scheme of the reactive deposition of AlN films. Adapted from [46]

The conventional reactive magnetron sputtering may comprise some problems with some materials, namely the poisoning of the target, which refers to the covering of the

target surface with the reaction product [41, 44], these problems can result in the origin of arcs. Arcing is characterized as intense, localized concentrations of plasma in contrast with an uniform and stable glow discharge needed for a stable sputtering process [47]. One way to overcome that problem is to use the pulsed mode magnetron sputtering [41].

Pulsed sputtering can be divided in the unipolar mode in which the negative target potential is switched to the ground potential or in the bipolar mode in which the potential is switched to positive [48].

The most common approach is the use of the bipolar mode with a "pulse-on" limited phase, so that the charging of the poisoned regions do not reach a critical point where arcing occurs [41], the "pulsed off" phase, corresponding to the temporally reverse voltage phase, allows the cleaning of the cathode with electrons, dissipating the charges through the plasma and allowing arc prevention, as shown in fig. 2.3 [41, 47].

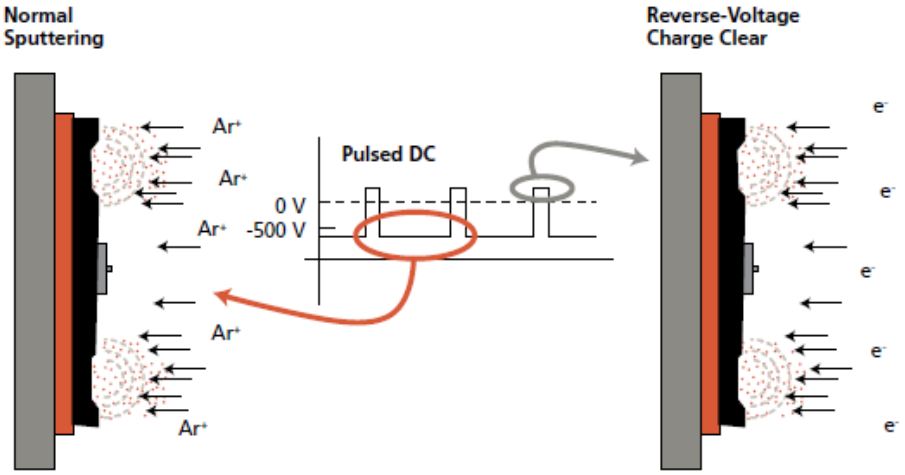

Fig 2.3 – Reverse voltage pulse modulation for active charge clearing and arc prevention [47]

2.1.3 Deposition equipment

The coatings presented in this thesis were performed using a Hartec semi-industrial deposition chamber with the dimensions of 40x40x40 cm^3. This equipment is placed at Department of mechanical engineering, University of Coimbra.

The system is basically composed by a vacuum system, a gas flow meter system, power supply alimentation system and the etching system (Kauffman Ion gun,fig 2.1). The target was operated in a Pulsed magnetron mode.

Fig. 2.4 shows a schematic representation of this deposition chamber.

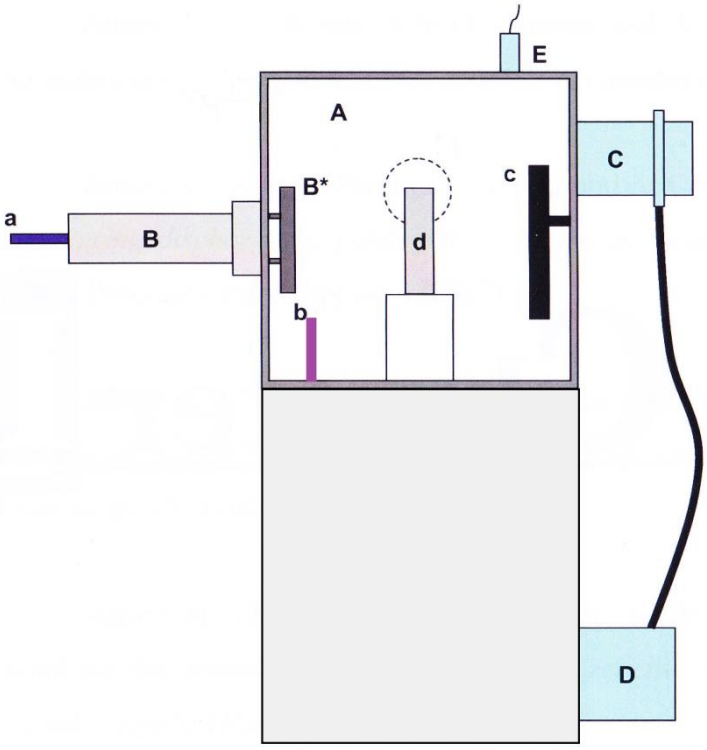

A – Deposition Chamber
B – Ion Gun
B* – Ion Gun accelerating electrode
C – Turbomulecular vacuum pump
D – Rotary vacuum pump
E – Pressure sensor
a – Argon inlet
b – Nitrogen inlet
c – Aluminum Target
d – Substrate holder

Fig 2.4 – Schematic representation of the HARTEC deposition chamber, adapted from [45]

2.2 Materials

2.2.1 Target and gases

In the films deposition a 15 cm x 15cm aluminum target was used (99,999% purity) and nitrogen (with different partial pressures) was used as reactive gas.

Argon was used as the inert gas (with different partial pressures between etching and deposition process).

2.2.2 Substrates

In this work, four different substrates were used: Silicon, Glass, Polyurethane (PU) and Polycarbonate (PC).

Silicon (100) and Glass were used due to its usefulness in film characterization; both polymers were employed because of the finality of the project, to serve as a cheap substrate for the development of the desired AlNx electrode.

Polyurethane was prepared with a constant mixing of an isocyanate prepolymer Biresin® U1419 and an amine hardener Biresin® U1419 in a proportion of 100:16 in a thermal bath at 70ºC [49]; after that, the hot mixture was quickly shed in a Teflon mould, and cooled at room temperature.

The polycarbonate used was a commercial PC-TECANAT [50].

Prior to the usage in the process, the above referred substrates were ultra sound cleaned:

Silicon and glass were washed in an ultrasound bath using ethanol and acetone for 10 minutes each.

Both polymers were ultrasound cleaned with 2-propanol and deonized water for 10 minutes each.

2.2.3 Coating procedure

The deposition process was performed as follows:

After reaching a ultimate base pressure normally better than $2{,}5 \times 10^{-3}$ Pa, the etching was performed using a argon pressure of approx. 0,22 Pa. The Kauffman ion gun grid system was set as I=13A (with a correspondent potential around 35-40 V) was obtained. The substrate bias was set as – 35 V.

Then, the Argon pressure was increased up to 0,55 Pa and nitrogen with several partial pressure ratios within [0,12 – 0,18] was added to the system in order to deposit aluminum nitride films with different nitrogen contents. The nitrogen partial pressure ratios were calculated using the relationship: $P_{N_2} = \frac{(P_{Total} - P_{Ar})}{P_{Ar}}$ [45].

After etching, the target was switched on and a delay time before the positioning of the samples in front of it was used. This delay time was used to allow the cleaning of the target, because of the poisoning of its surface inflicted by the aperture of the chamber and its exposition to atmospheric ambient.

A power of 500 W was applied to the target (with a f=250 Hz and a t_{on}= 1600 ns); the substrate-to-target distance was 65 mm, and there was no substrate Bias.

The same pumping speed was used for the etching and on all the deposited films.

Due to the insertion of a thermocouple in the polymers for the monitoring of the temperature achieved on its surface, both the etching and the deposition were performed in a static mode.

Tables 2.1 and 2.2 summarize the conditions used for the experiments

Table 2.1: Summary of the Etching conditions/parameters

Etching conditions	Value
Base Pressure	$<2,5x10^{-3}$ Pa
Argon pressure	0,22 Pa
Kauffman Ion Gun current	13 A*
Substrate Bias	-35 V
Etching Time	1/2/4 min*

***These conditions must be consired only for the Polycarbonate treatment**

Table 2.2: Summary of the Sputtering conditions/parameters

Sputtering conditions	Value
Base Pressure	$<2,5x10^{-3}$ Pa
Argon partial pressure	0,55 Pa
Nitrogen partial pressure ratio	$0,12<P(N_2)/P(Ar)<0,18$
Target Power Supply	500 W
Substrate Bias	Floating
Deposition mode	Static (without substrate rotation)
Target to substrate distance	65 mm
Deposition time	3min

2.3 Characterization Techniques

Several characterization techniques were taken in order to study and understand both the etching effects and the coating properties.

Tables 2.1 and 2.2 summarize these techniques and the properties measured while using them.

Table 2.3 – Etching characterization techniques

Technique	**Property**
Contact Angle Measurement	Wettability
Atomic Force Microscopy	Roughness

Table 2.4 – Thin film characterization techniques

Technique	**Coating characterization**
Profilometry	Thickness
SEM/EDS	Chemical composition /morphology
4 probe method	Resistivity
X-Cut tape test	Adhesion
X-Ray diffraction	Structure
Nanoidentation	Hardness

2.3.1 Contact Angle

There is no available method to directly measure a solid surface energy; instead, it is possible to measure the contact angle (C.A.) of the dispersion of a liquid drop on a solid surface, and infer about the surface energy [51]; this method is known as the sessile drop method, and it is the most widely used method to measure this parameter [52, 53].

The static contact angle is captured when the drop reaches a thermodynamic equilibrium [54]. A surface in which a water drop makes a C.A. over 90º represents a surface with a low free energy and poor adhesiveness, while a surface with a water drop C.A. less than 90° represents a hydrophilic surface (fig. 2.5) [54, 55].

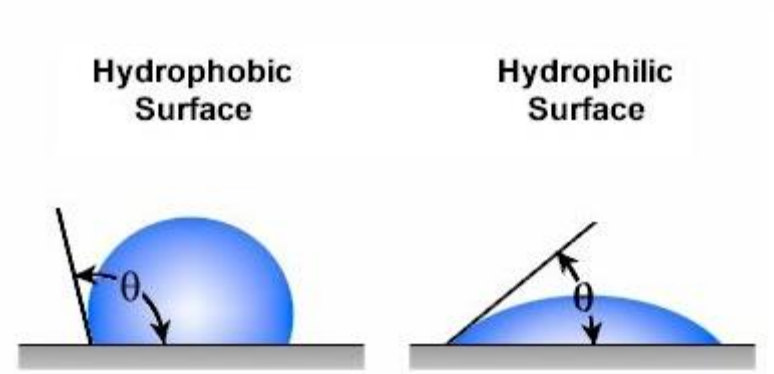

Fig 2.5 – Contact angles for two surfaces: hydrophobic and hydrophilic [51]

In this work, for the static C.A. determination, a micrometric volume of a deonized water drop was vertically syringed in the polymeric samples and a photo was taken in order to determine the degree of the drop's dispersion, as shown in fig 2.6. The photos taken were analyzed using the Image J software (U. S. National Institutes of Health, Bethesda, Maryland, USA) with the Drop Snake plug-in [56], which allows obtaining the contact angle value from the camera photo.

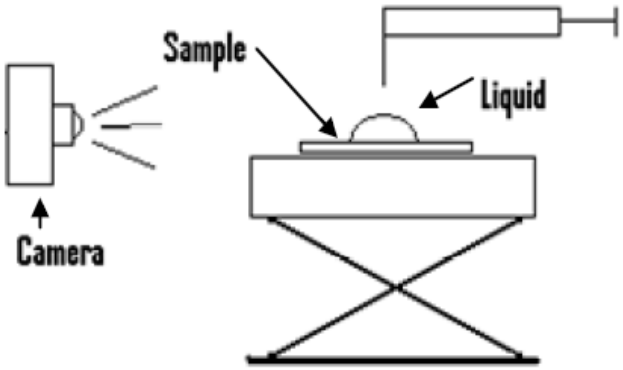

Fig. 2.6 – Contac angle measuring system, adapted from [46]

This procedure was used both for the pre-etching sample and for samples with three different times of treatment, in order to determine any pattern evolution of the contact angle.

2.3.2 Atomic force microscopy

The principle of atomic force microscopy (AFM) relies on the interaction of a sharped probe, placed on the extremity of a cantilever, with the sample surface. Due to the interatomic forces between the probe and the surface, the cantilever deflects proportionally according the Hooke Law:

$$F = -K * x \qquad \text{(equation 2)}$$

in which F represents the atomic force, K is a constant of the cantilever material and x represents the deflection.

By coupling a laser beam, the cantilever's deflection is detected and collected in a photodiode; this is divided in four parts, allowing the construction of a topographic map due to the position and intensity of the beam over the four quadrants [43].

Among the parameters provided by AFM, average roughness (Ra) is the most assessed. Ra is determined from the arithmetic mean of the height deviation from the surface in respect to an average line profile. [43].

For this assay, the Innova® Atomic Force Microscope (Veeco, Bruker, USA) was used. A 10x10 μm^2 area was scanned, with a resolution of 512 lines and a frequency of 0,6 Hz in contact mode. This procedure was repeated five times within a 100x100 μm^2 area, and the data were analyzed using Gwyddion (Czech Metrology Institute, Czech Republic) in order to obtain the average roughness and topographic views of the polymeric surfaces.

2.3.3 Profilometry

Profilometry consists in the measurement of the step between the substrate and the film surface. This step is intentionally created by the addiction of a small drop of boron nitride on the substrate before deposition, which is easily removed after the process, allowing the measurement of the film's height: the scan determines the ledge between the film and the substrate [52].

The equipment used to perform this test was Mahr Perthometer PGK w/S4P (Mahr GmbH, Göttingen, Germany).

2.3.4 Scanning electron microscopy

Scanning Electron Microscopy is a technique which allows the study of several film features as coating morphology, thickness and composition [43].

The scanning microscope is basically composed by a vacuum chamber, a tube where electrons are accelerated, a secondary electron detector and a backscattered electron detector (fig 2.7) [57].

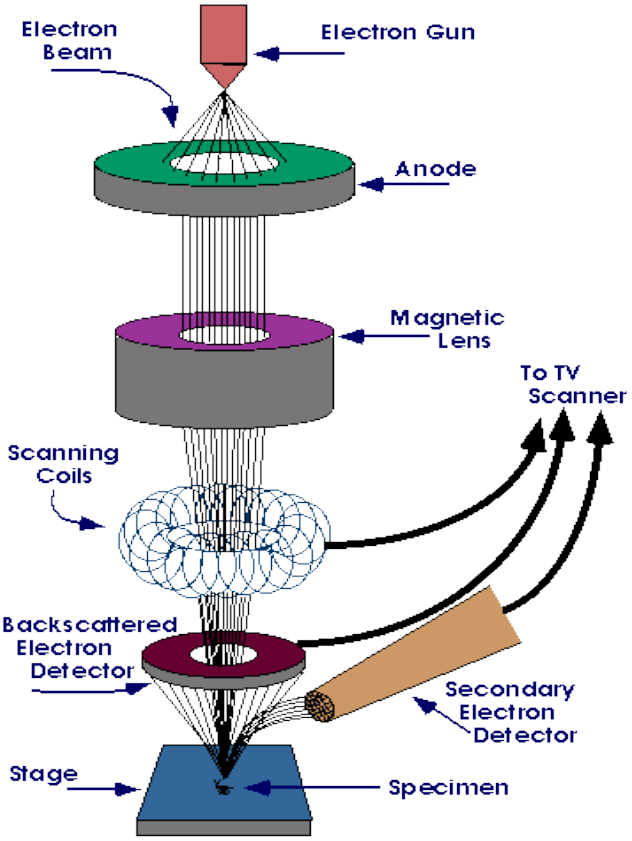

Fig 2.7 – Scanning Electron Microscope scheme [57].

With an applied voltage, the electrons emitted by the cathode are accelerated towards the anode. Through an optic system, composed by a condenser lent and an objective lent, it is possible to focus the electron beam with high precision. Then, the beam passes through several scanning coils which deflect the beam horizontal and vertically in order to scan a specific sample area [42, 43].

When the beam interacts with the sample, the electrons loose their energy by dispersion and absorption, resulting in the emission of secondary electrons which will be collected in the above referred detectors [42]. In these detectors the signal is amplified due to a photomultiplier tube, generating an electric signal which produces the SEM image [42, 57].

Film's chemical composition was obtained with a Jeol JSM-6300 Scanning Electron Microscope (JEOL Ltd., Tokyo, Japan), while morphology images were assessed with a NanoSEM – FEI Nova 200 (FEG/SEM) (FEI, Oregon, USA).

2.3.5 X - Ray diffraction

X-ray difraction (XRD) is a non destructive technique used to determine the crystalline structure of the deposited films [42].

A polycrystalline structure is constituted by several crystals which present a structural order and each one is organized in small coherent diffraction domains separated by dislocation networks; in each coherent domain it is possible to establish atomic planes separated by an interplanar distance d_{hkl}. These planes are characterized by a high atomic and thus electronic density, so that when a crystalline material is irradiated with an X radiation, it has the ability to diffract the incident radiation if it is in the same order of the interplanar distances of the crystalline structures (fig. 2.8). This phenomenon can be analyzed using the Bragg law:

$$2\, d_{hkl} \sin\theta = n\, \lambda \quad \text{(equation 3)}$$

This law relates the diffraction angle (θ), the X - Ray wave length (λ) and the interplanar distance of the crystals (d_{hkl}) [43, 52].

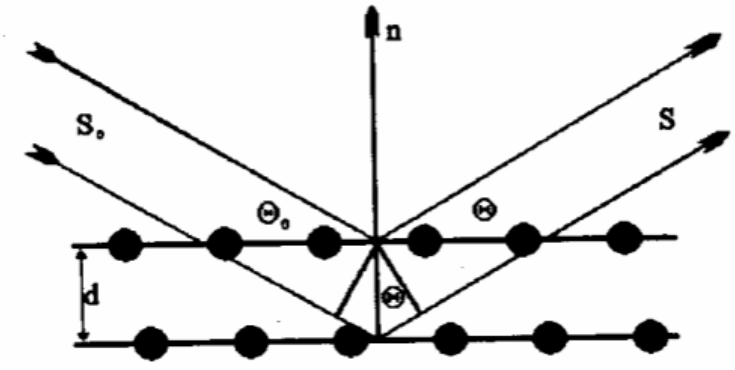

Fig. 2.8 – Scheme of the interplanar diffraction phenomena [42].

The diffracted beams are detected and its angles are read and processed, then it is possible to make an approach to the crystalline structure of the material [42].

The assays were performed in a PANalytical X'Pert diffractometer (PANalytical, Almeno, the Netherlands), with grazing incidence.

2.3.6 Adhesion

Thin films' adhesion was evaluated using the X-Cut tape technique, according to the ASTM standard D 3359-08. This technique consists on the application and removal of a sensitive adhesive tape against the coated film. Since an intact film with normal adhesion is normally not removed, the accuracy of the test is usually improved by cutting into the film a figure X or a grade hatched pattern, before the application of the tape. After the tape is pulled off, the resistance and/or the degree of film removal is assessed by optical microscopy, and quantified by the comparison with an established rating scale [58].

2.3.7 Nanoindentation

The hardness assays consist in the application of a load, in an indentator, which acts in the sample plane surface. The determined hardness is the ratio between the maximum load value applied during the assay (P_{max}) and the contact area between the indentator and the sample in the beginning of the download, projected in the sample surface (A_c) [52].

$$H = \frac{P_{Max}}{A_C} \qquad \text{(equation 4)}$$

To obtain the Ac value, it was used the formula:

$$A_C = A + B * h_C + C * {h_C}^2 \quad \text{(equation 5)}$$

with hc corresponding to the plastic deformation depth and the rest of constants were determinate using calibration tests. Through these values it is possible to obtain the films' elasticity modulus (E), using the reduced elasticity modulus (E_r):

$$\frac{1}{E_r} = \frac{1-\nu^2}{E} + \frac{1-{\nu_i}^2}{E_i} \qquad \text{(equation 6)}$$

where E_i is the indentator elasticity modulus, ν and ν_i correspond to the Poisson coefficients of sample and indentator, respectively [52].

The equipment used for these measurements was a MicroMaterials NanoTest (Micro Materials, Wrexham, UK).

2.3.8 Four probe method

Surface resistivity is the material's inherent resistance to current flow; and does not depend on the dimensions of the material [59].

The four probe method was the technique used to determine the films' surface resistivity. This method, one of the most common surfaces resistivity measuring methods, uses four probes aligned linearly or in a square pattern that are in contact with the surface of the test material [59], then current is passed through two of these probes, and the potential drop is measured on the other probes, generally the outer probes are used for the current passage while the inner are employed in the potential measurement (fig 2.9) [60].

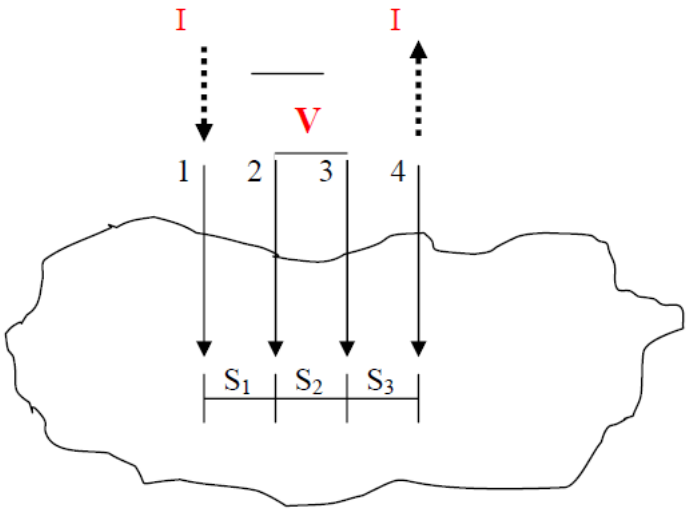

Fig. 2.9 – Four probe test setup. Probes 1 and 2 carry current while probes 2 and 3 measure voltage [59]

If the distances S1, S2 and S3 are equal, the surface's resistivity can be given by:

$$\rho = 2 * \pi * S * \frac{V}{I} \qquad \text{(equation 7)}$$

When it is intended to perform a measurement on a finite sized area, some correctional factors must be considered [59, 60]. These factors are dependent on the sample thickness, edge effects, and the position of the probes on the sample among others [59]. For the measurements carried during this work, and attending to these factors the used formula was:

$$\rho = 2 * \pi * \ln(2) * \frac{V}{I} * t \qquad \text{(equation 8)}$$

In which t means the films' thickness and $\ln(2)$ corresponds to the correctional factor.

Chapter 3
Results and discussion

3.1 Coating of AlN_x on silicon and glass

3.1.1 Achievement of the desired x value range

During the first set of depositions, it was intended to study the system in order to obtain films with the desired features. Thus, the nitrogen partial pressure ratio was narrowed down from conductive and insulating films (confirmed using a multimeter) to intermediate ones. Deposition rates and, in a later stage, film's hardness and resistivity were calculated. Silicon and glass were used as substrates.

3.1.1.1 Target Potential and Deposition Rate

The evolution of the target potential as function of the nitrogen partial pressure ratio is plotted in fig. 3.1. This discharge curve was obtained by varying the nitrogen flow during the same experiment, in which the target potential measurements were acquired with a delay time between each flow variation in order to allow the system to reach a stable regime.

From fig 3.1 it is possible to notice an almost linearly smooth target potential decrease with a nitrogen partial pressure ratio increase up to 0,16, varying from 247,1 V (P_{N2}/P_{Ar}=0,12) to 233V (P_{N2}/P_{Ar}=0,16). After that, a more accentuated decrease was observed, with an obtained target potential of 208 V for a correspondent nitrogen partial pressure ratio of 0,18.

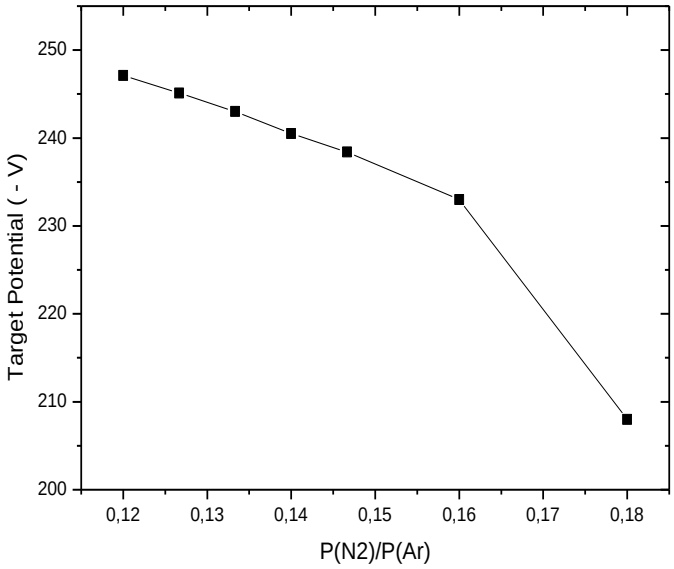

Fig. 3.1 – Evolution of the target potential as function of N_2 partial pressure ratio.

The first linear target potential decrease trend is related with a higher ionization probability (Ep) provided by the nitrogen density increase. This higher Ep is reflected in a lower value of minimum target potential (Vmin) to sustain the discharge, since $V_{min} \propto 1/Ep$ [61]. Nevertheless, in a reactive sputtering system, besides the reactive gas interaction with the sputtered material, there is also its reaction with the cathode surface [41, 62, 33]. For higher reactive gas partial pressures, this interaction leads to the covering of the cathode with the reaction product (target poisoning) [41, 33] which is characterized by a significantly decrease of target potential [61]. For the AlN binary system, a total target covering occurs for a P_{N2}/P_{Ar} of approximately 0,20 [33], thereby it is possible to assume that for partial pressure ratios higher than 0,16 an almost covered target mode was obtained with the consequence of an abrupt drop of potential.

Concerning the deposition rate, from the analysis of fig. 3.2 one can notice a trend that is similar to the target potential evolution as a function of nitrogen partial pressure ratio increase. Indeed, for P_{N2}/P_{Ar} higher than 0,16 the same accentuated drop (75,5 nm/min for P_{N2}/P_{Ar} = 0,16 and 48,4 nm/min for P_{N2}/P_{Ar} = 0,18) was observed. This behaviour is related with the decrease of the sputtering yield - the average number of atoms removed from the

target per incident ion [36] - as a consequence of the cathode's surface poisoning in response to the reactive gas pressure increase [61].

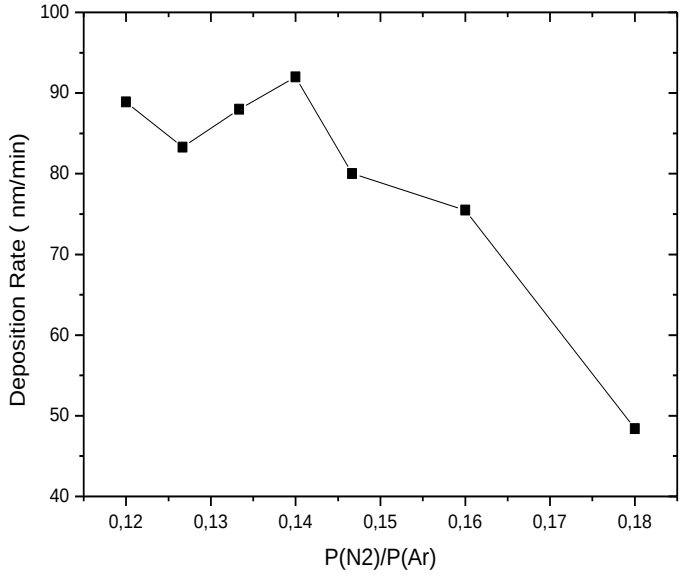

Fig. 3.2 – Evolution of the deposition rate as function of N_2 partial pressure ratio

Within the zone with nitrogen partial pressure ratios between 0,12 and 0,16 (89,9 nm/min and 80 nm/min of deposition rate, respectively) a smooth decrease in deposition rate was expected, in accordance with the target potential values obtained for the same range of nitrogen partial pressure ratios.

The unexpected lower/ higher deposition rates obtained for P_{N2}/P_{Ar} =0,127 (83,3 nm/min) and P_{N2}/P_{Ar} =0,14 (92,0 nm/min) in respect to a linear fit plotted between the two extremes of the considered range should be understood as non-representative, since they represent a deviation inferior to 5 %. Thus, they have to be related with some possible lack of accuracy provided by the deposition rate analysis method (Profilometry), since the deposition rate is expected to decrease continuously with the increase of nitrogen partial pressure ratio [33].

3.1.1.2 Hardness

The hardness and Young's modulus values were assessed recurring to nanoindentation for films with thickness beyond 1 micron.

Both the hardness and the reduced Young's Modulus have increased with the increment in the nitrogen partial pressure ratio from values of 8,27 Gpa (hardness) and 135,8 GPa (reduced Young's modulus) for P_{N2}/P_{Ar} = 0,12 to values of 11,6 Gpa (hardness) and 164,8 (reduced Young's Modulus) for P_{N2}/P_{Ar} = 0,147 (fig. 3.3). The observed continuous increase of hardness and reduced Young's modulus with the increase of nitrogen partial pressure (for depositions in which all the others parameters are kept constant) led to the assumption that nitrogen content has important implications on the obtained hardness and reduced Young Modulus values.

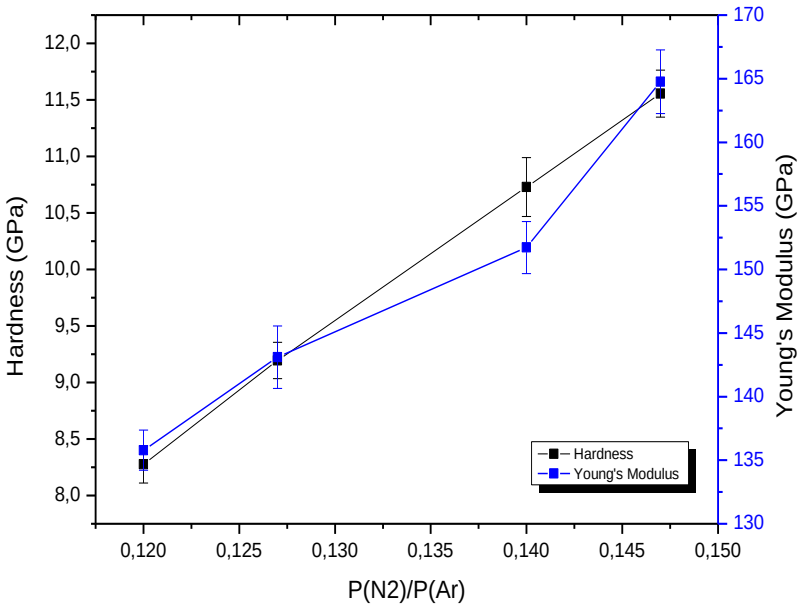

Fig. 3.3 – Hardness and reduced Young Modulus Values as function of nitrogen partial pressure.

A thin film hardness can be altered by changes on its microstructure and/or residual strains [33]. The hardness and reduced Young's modulus increase observed in fig. 3.3 is caused by the lattice distortions introduced by nitrogen [63, 64]. Indeed, during the deposition nitrogen is placed in the Aluminum lattice interstices leading to its dilatation, which induces compressive stresses, increasing films' hardness [64]. As more nitrogen content is deposited, a bigger effect is verified.

The film deposited with the higher P_{N2}/P_{Ar} (0,147) presents a hardness value within the hardness range considered for the bulk AlN (table 1.2). From the observed hardness increase trend, it is expectable a higher hardness for a stoichiometric AlN film when compared to the bulk material. This discrepancy is also related with the above referred stresses induced during deposition [33].

3.1.1.3 Resistivity

Film's resistivity was determined (for films 200 – 300 nm thick) using the four probe method, at room temperature. Fig. 3.4 shows the film's resistivity as function of nitrogen partial pressure ratio.

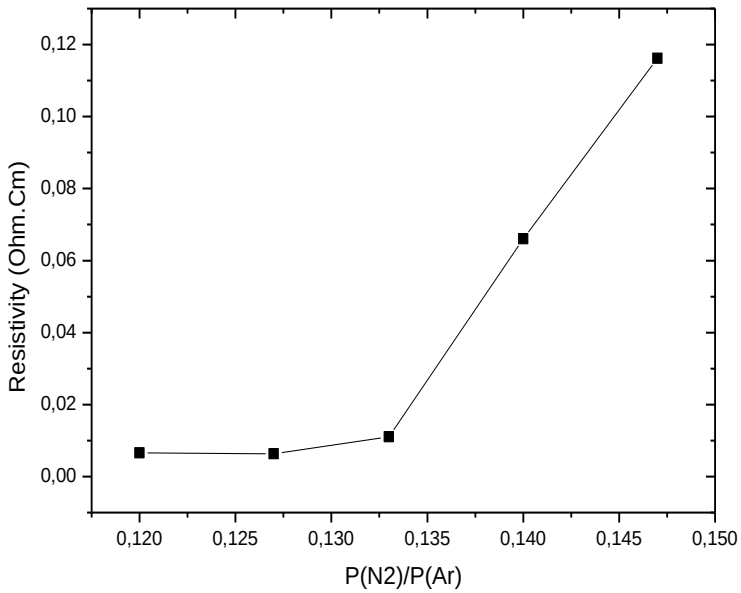

Fig. 3.4 – Electrical Resistivity, measured at room temperature, as function of nitrogen partial pressure ratio.

Regarding fig. 3.4, it is possible to notice a smooth resistivity increase with the increase of nitrogen partial pressure ratio from 0,12 up to 0,133, with the obtained values ranging from $6{,}6\times10^{-3}\Omega$.cm to $1{,}1\times10^{-2}$ Ω.cm; after which a more accentuated increase is observed, with a obtained resistivity of $1{,}17\times10^{-1}$ Ω.cm correspondent to P_{N2}/P_{Ar} =0,147. These values are in good agreement with the expected ones for the nitrogen content (calculated below) correspondent to this nitrogen partial pressure ratios range [33].

A material's electrical resistivity is primarily determined by its intrinsic properties, defects and temperature [63]. The latter factor had not importance on the observed trend, since the measurements were all performed at the same temperature (room temperature).

For the reasons previously explained for the hardness increase, it is possible to conclude that also here the film's nitrogen content played an important role for the verified electrical resistivity increase. In fact, the increase of nitrogen content leads to a change in the phase composition [63] which is assumed to be more likely conductor for lower nitrogen partial pressure ratios, and more likely insulating for higher P_{N2}/P_{Ar}.

One may assume that the lattice defects introduced by nitrogen [63, 64] may comprise an enhanced importance for nitrogen partial pressures higher than 0,133.

3.1.2 Detailed analysis to the AlN_x films within the wanted resistivity range

Upon determination of the resistivity as function of nitrogen partial pressure ratio (fig 3.4), it was possible to infer a P_{N2}/P_{Ar} range of interest ($0{,}133 \leq P_{N2}/P_{Ar} \leq 0{,}147$). This range underwent a more detailed study in terms of chemical composition, structure and morphology.

Two sets of films were deposited, depending on the intended characterization. Thus, films with more than 1 μm of thickness were deposited (during 15 minutes) in order to evaluate the chemical composition and structure (due to equipment limitations, thinner films are not well characterized), while films with 200-300 nm were deposited (during 3 minutes) for the morphology characterization.

3.1.2.1 Chemical composition

Table 3.1 – Chemical composition of films for two N_2 partial pressures ratios.

P (N_2) /P(Ar)	N (%)	Al (%)	Ar(%)	Designation
0,133	36,3	59,1	4,6	1
	37,9	57,6	4,5	2
0,147	38,0	57,3	4,7	3

For simplicity of explanation, numbers were given to the films in this table.

The evaluation of chemical composition for the three previous referred N_2 partial pressure ratios was intended. However, unwittingly, two measurements were made for two films deposited with the same P_{N2}/P_{Ar}.

A higher nitrogen content is observed for the film with P_{N2}/P_{Ar}= 0,147 (38,0%) compared to the film deposited with lower nitrogen partial pressure ratio (36,3 % or 37,9%).

Indeed, the nitrogen content is expected to increase continuously as P_{N2}/P_{Ar} is increased up to 0,20. This behaviour is related with the target poisoning. With the increase of nitrogen partial pressure, the target is continuously covered with an AlN_x layer with the consequent deposition of films with higher nitrogen contents [33].

However, the measuring mistake led to the assumption that films' composition within this such small range of N_2 partial pressure ratios can vary "significantly" and chemical compositions differences are rather dependent on deposition conditions (as base pressure, or target previous poisoning) than films considered for a larger P_{N2}/P_{Ar} difference.

In fact, regarding the nitrogen atomic content for the film 2 in the table, its atomic difference in relation to the film 3 (0,1%) is inferior to the difference in relation to the film 1 (1,6%), what should not have occurred since films 1 and 2 were deposited under the same P_{N2}/P_{Ar}, whereas film 3 was deposited with a higher N_2 over Ar fraction.

It is possible to assume that for this rather small range of nitrogen partial pressure ratios, the nitrogen atomic content for a given P_{N2}/P_{Ar} may overlap the expected one for a higher nitrogen partial pressure ratio.

For the two compositions referred to the 0,133 nitrogen partial pressure ratio (films 1 and 2), different ultimate base pressures were used: $2{,}4 \times 10^{-3}$Pa for the film 1 and $2{,}2 \times 10^{-3}$ Pa for the film 2. Also the target potential, which was stabilized before placing the silicon substrate in front of the target, varied during the deposition.

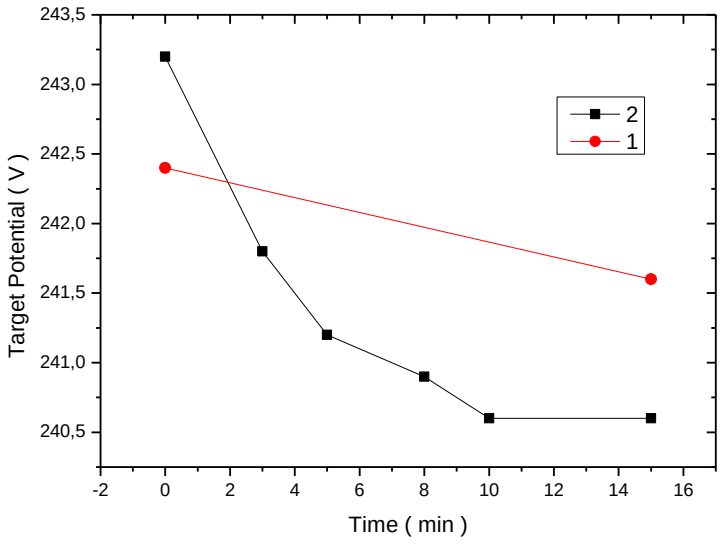

Fig 3.5 – Target potential evolution during the depositions of the films 1 and 2 (table 3.1).

From fig 3.5, the higher N_2 content obtained in film can be explained by the target potential evolution during the deposition. Indeed, during the major time of deposition, the target potential was substantially below the target potential of the deposition of film 1. Although for the film 1 the target potential was measured only in the beginning and in the end of deposition, its value is not expected to increase during deposition. Thus, even if it has reached its final value (241,6V) shortly after the beginning of the deposition, the target potential for the film 2 was inferior during the majority of the deposition time.

The lower target potential may indicate a higher target poisoning, with consequent higher nitrogen content in the deposited films. This target potential variation can be related with a different delay time in the target cleaning before the deposition for the two films and/or with the instability inflicted in the stable plasma with the substrate holder rotation (in the beginning of the deposition, for the placement of samples in front of the target).

Nevertheless, it must be pointed out that within the considered small range of nitrogen partial pressure ratios, this possible overlapping of nitrogen contents can be consequence of reactive sputtering limitations, regarding its several inter-connected parameters. However, regarding the obtained values, an x value range (0,613 to 0,655) was determined.

3.1.2.2 Structure

Coating's structure characterization was evaluated using X-Ray diffraction (XRD). Fig 3.6 shows the x-ray diffraction patterns for the considered nitrogen partial pressure ratio.

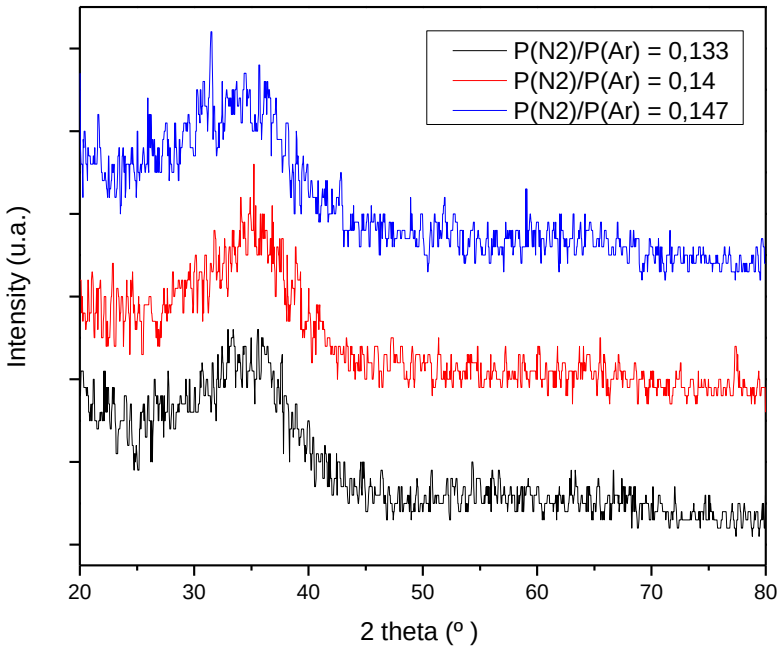

Fig 3.6 – X –Ray diffractogram patterns of the defined N_2 partial pressure ratios.

From the analysis of fig. 3.5, one can observe that films are amorphous, presenting (all) broad peaks in the range of $30<2\theta<40º$.

For the deposition of the Al-N binary system, varying the nitrogen partial pressure ratio, different patterns of X- Ray diffraction can be obtained. Indeed, for $P_{N2}/P_{Ar} = 0$,

peaks correspondent to the face-centered cubic (f.c.c) structure of aluminum (Al(111) and Al(200)) are observed [33, 65]. With the nitrogen partial pressure ratio increase, the characteristic aluminium diffraction peaks are expected to disappear [65] indicating a grain size reduction and a tendency for structure amorphization [33].

For a N_2/Ar relation high enough to promote a stoichiometric film formation, the observed peaks correspond to the hexagonal compact (h.c) structure of aluminum nitride [33, 65].

Regarding the intermediate zone of nitrogen partial pressure ratios, the characteristic amorphous structures may present low intensity diffraction peaks precursors of the characteristic AlN hexagonal structure peaks [65].

The obtained broad peaks (fig. 3.6) may, thereby, be indexed to the hexagonal structure of AlN, in which their unexpected higher intensity can be related with the conditions of deposition. Indeed, an increase in deposition power has already been proved to impose a crystalline arrangement for a previously amorphous structure deposited under the same other sputtering conditions/parameters [33, 66].

The depositions concerned to fig. 3.6 were carried out during 15 minutes (fig 3.5) at a constant target power of 500W in static mode, thus, these conditions could be enough to promote an increase in the expected low intensity broad peaks for this nitrogen content range [65]; for these reasons and from their position ($2\theta \approx 35^{o}$), these broad peaks may be indexed to the plane (002) of the AlN hexagonal structure, since a high sputtering power is advantageous for the growth of AlN with this orientation [33, 65].

3.1.2.3 Morphology

Films´ morphology was assessed using Scanning Electron Microscopy. AlN_x films, due to their lower conductivity, were recoated with a 20-30 nm layer of gold. Figure 3.7 shows film's morphologies for the three considered nitrogen partial pressure ratios.

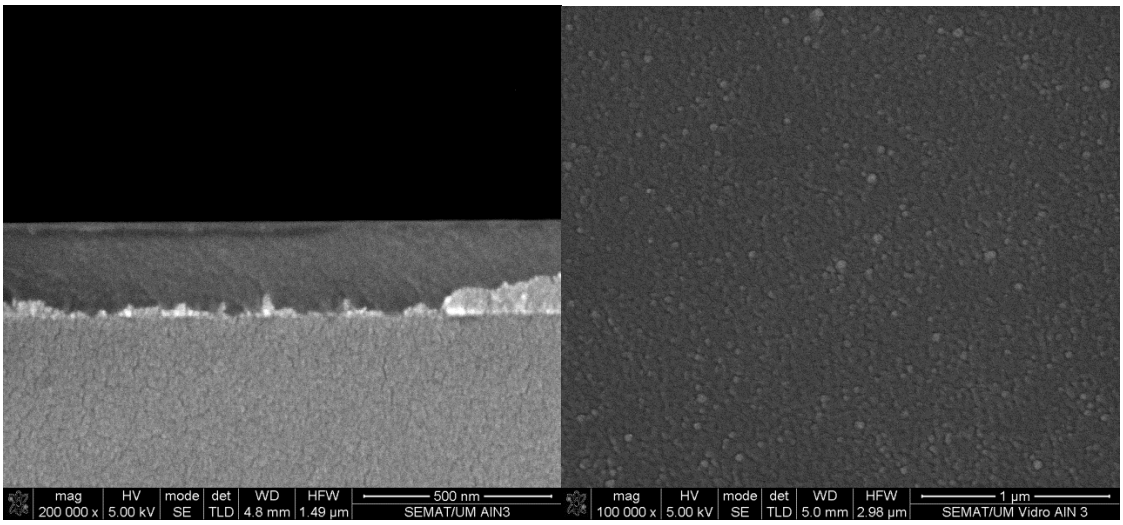

Fig 3.7 a) Cross section and Top view of a AlN_x thin film deposited with P_{N2}/P_{Ar} = 0,133

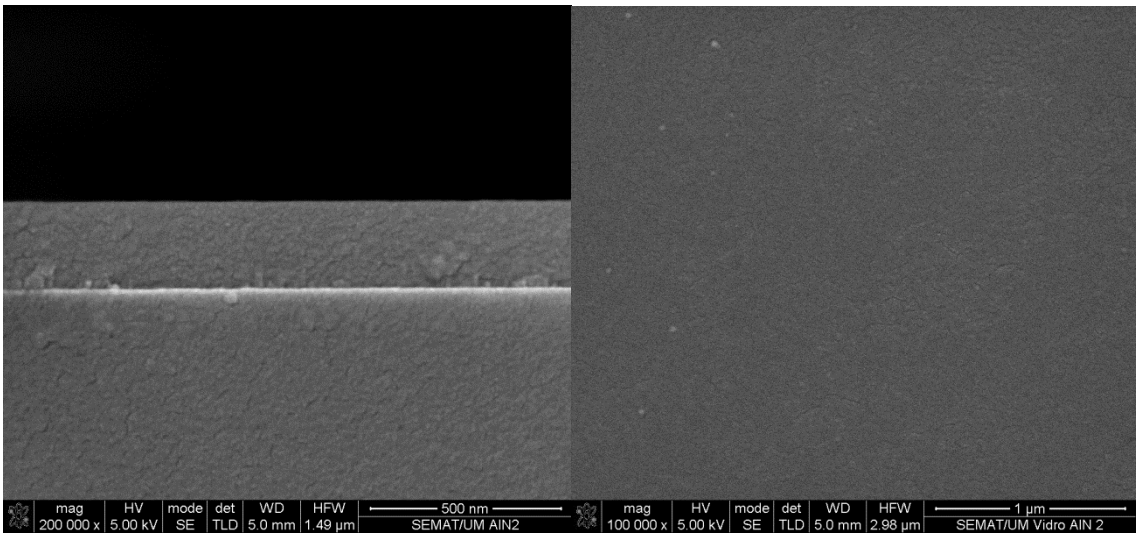

Fig 3.7 b) Cross section and Top view of a AlN_x thin film deposited with P_{N2}/P_{Ar} = 0,140

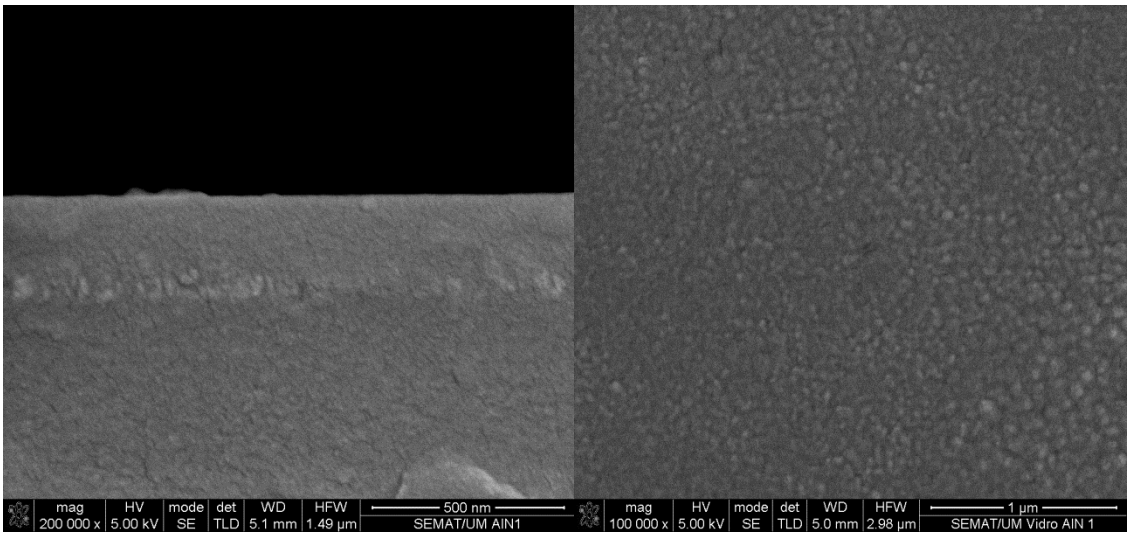

Fig 3.7 c) Cross section and Top view of a AlN_x thin film deposited with P_{N2}/P_{Ar} = 0,147

From the cross section analysis it is possible to observe a feature-less dense growing in all the films. From a detailed inspection to the top views of films with nitrogen partial pressures of 0,133 and 0,147 (the P_{N2}/P_{Ar} extremes of the considered range) a granular morphology is observed, which may indicate a columnar growing (Fig. 3.7a,c). The observed smooth surface morphology for P_{N2}/P_{Ar} = 0,140 (Fig. 3.7b) has to be considered as non-representative since films' characteristics should be similar within such small range of nitrogen partial pressure ratios, as observed for chemical composition and X-ray diffraction. Thus, it must be associated with some unexpected event during deposition, or to an inefficient glass etching. Indeed, the glass substrates underwent the same etching as the polymeric samples (shown later), which by some reason might have not been enough for a good surface cleaning of the sample correspondent to the film with P_{N2}/P_{Ar} = 0,140 possibly contaminated during its transportation from the sample preparation room to the deposition chamber.

Concerning the film growing, and taking into account the obtained data with the X-Ray diffractrogram patterns for this nitrogen partial pressure ratios and the granular surface topography of the films, a not well defined columnar structure must be expect [66]. This not well defined columnar structure is not observed in the cross sections possibly due to some mask effect provided by the glass substrate.

3.2 AlNx coating of polyurethane

Whereas in the previous sub-chapter both films with 200-300 nm and films over 1 micron of thickness were deposited, depending on the intended characterization, here, as well as in the next sub-chapter (3.3), only 200-300 nm thick films were deposited, within the composition range defined in 3.1.1.3. For this purpose, and taking into account the deposition rates (3.1.1.1), a time of 3 minutes was set for the depositions.

From the previous knowledge concerning the difficulty of achieving a good adhesion when depositing a film onto polyurethane, when the film and substrate display very different thermal expansion coefficients, [60], a thermocouple was embedded in the polyurethane in order to follow the temperature evolution during both the etching and deposition steps. This monitoring could lead to a better control of the etching/sputtering conditions [67] in order to avoid film crack formation, and thus improve the quality of the coatings.

When used, the thermocouple showed to be affected by the magnetic field of the target power supply, displaying an incorrect temperature measurement, and thus preventing a temperature monitor during deposition. However, it had a great usefulness to understand the effects of the etching Kauffman ion gun, as shown next.

3.2.1 Normal temperature evolution for the 200-300nm AlN_x films

Fig 3.8 shows the temperature evolution during the entire deposition process of the AlN_x thin films onto Polyurethane.

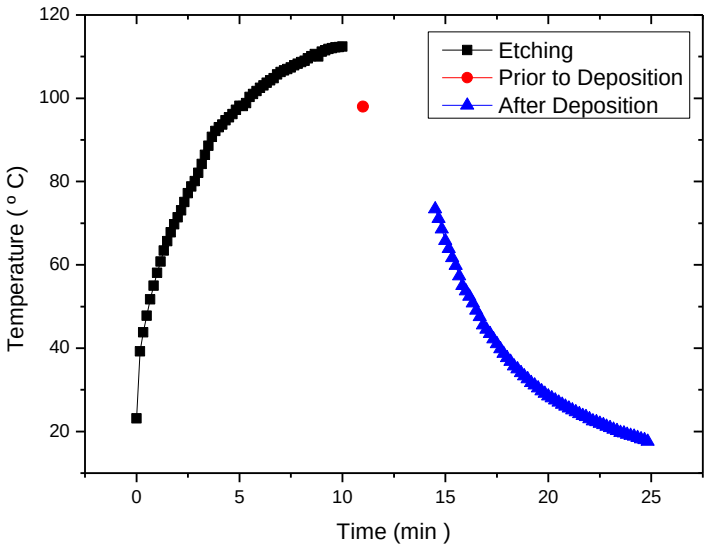

Fig. 3.8 – PU Surface temperature measured during the entire process

During the plasma etching treatment (10 minutes), the temperature increased beyond 110ºC, decreasing to 98ºC one minute after the end of the etching, after which the deposition (3 minutes) has started. The temperature was measured again immediately after deposition. The acquired values showed a lower heating power of the target power supply in relation to the Kauffman ion gun, with the film deposition occurring under a temperature decrease (from 98 ºC to 73,4 ºC).

From fig 3.8, it is also possible to notice a relatively high cooling rate after deposition. This fact is explained by the attachment of polyurethane directly onto the substrate-holder, so that after the treatment heat releasing could occur through the copper (of which the substrate holder is composed).

3.2.2 Polyurethane Substrate failure

Fig 3.9 shows the film crack differences for films deposited onto samples placed in different positions over the substrate holder, during the same deposition.

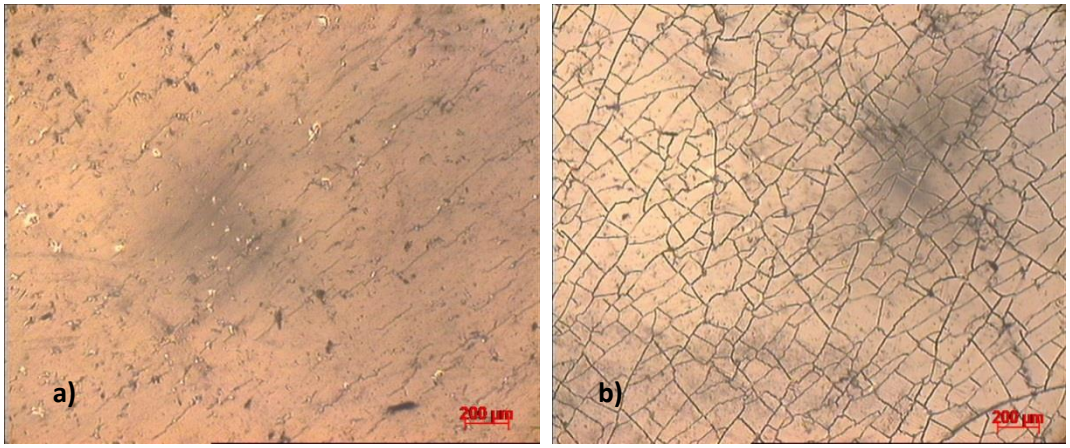

Fig. 3.9 – Crack formation mechanism differences for samples in the same deposition.

From fig 3.9, one can observe a significant difference between both samples. Fig 3.9 a) shows a sample positioned in the center of substrate holder, while the fig 3.9 b) shows a sample placed far from it.

It is possible to distinguish a more abraded surface, fig 3.9 a), and a surface with a more defined film crack, (fig 3.9 b). Nevertheless, in both samples it is possible to notice a surface damage, which was associated with the ionic bombardment during etching. Samples were exposed to etching during 10 minutes, while the film deposition was carried during 3 minutes, furthermore etching proved to be more powerful in terms of heat transferred to the substrate, fig. 3.8. These data suggested an anisotropic effect of the Kauffman Ion gun, which was confirmed by literature findings [36], and an excessive etching time treatment.

The appearance of film crack was related with the conjunction of the mechanical properties of the thermoset Polyurethane and its small thickness. Indeed, when heated (using a heating plate) PU showed a visible deflection (even for relatively low temperatures). Inside the deposition chamber its behaviour under etching/deposition conditions should mimic the observed one with the heating plate, thus the growing AlN_x thin film, inevitability undergoes a crack formation during deposition, where according to fig 3.8 these crack formation mechanism should be due to compression [68], since a

diminishing of PU curvature with the temperature decrease is expected. Thus, polyurethane proved not to be suitable to act as substrate for film growing.

3.3 AlNx coating on polycarbonate

As polyurethane showed to be unsuitable to act as substrate, it was replaced by a thermoplastic polymer – polycarbonate.

3.3.1 Circumscription of a working zone

Given the observed anisotropic effect of the etching system, it was decided to perform a detailed study of its effects on the temperature attained by the polymer's surface, in order to find a homogeneous work zone. This study comprised a temperature achievement as function of the sample's position over the substrate holder, as well as a temperature achievement as function of the current on the extraction grid system of the Kauffman Ion gun (which was vaguely observed during the polyurethane coatings).

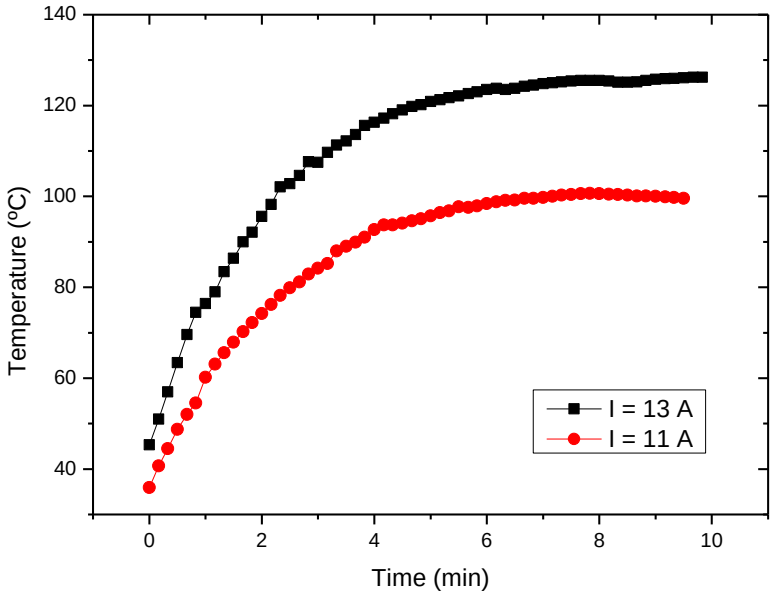

Fig 3.10 Temperature attained on PC substrate for two different etching currents

Firstly, for substrates placed in a fixed position over the substrate holder, a temperature study as function of the current on Kauffman ion gun was performed. As it is possible to notice from fig. 3.10, the higher the current, the higher the attained temperature on polycarbonate was.

From this assumption, a study of temperature dependence with sample position on substrate holder was carried. For this purpose, three thermocouples were inserted inside the chamber. Given the verified temperature dependence on the current in the ion gun, low currents were used (in order to reach a lower temperature on polycarbonate surface). Some obtained plots, with the respective samples' assembly schemes, are shown below.

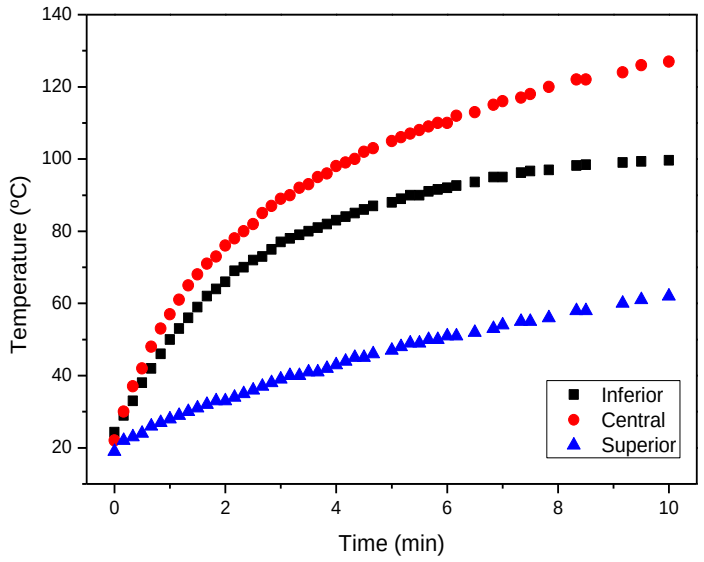

Fig. 3.11 a) PC temperature as function of sample position on the substrate holder for a current of 10 A.

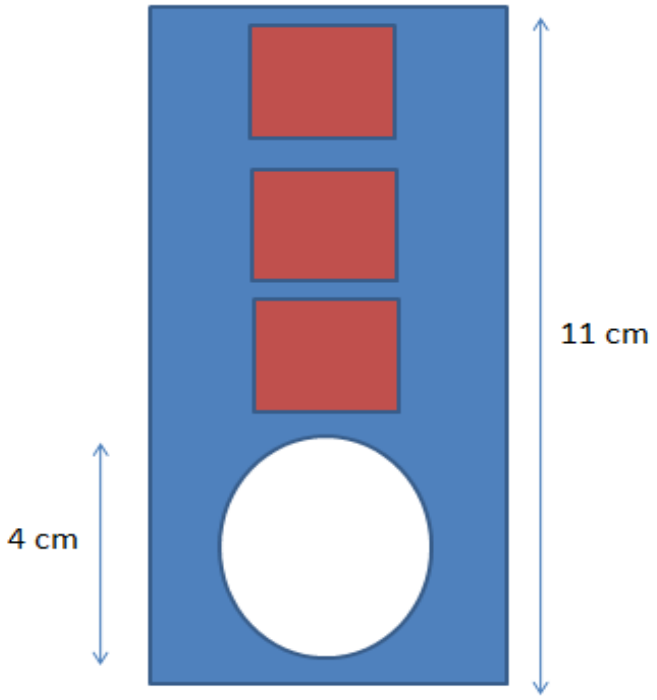

Fig. 3.11 b) PC samples assembly correspondent to the previous figure.

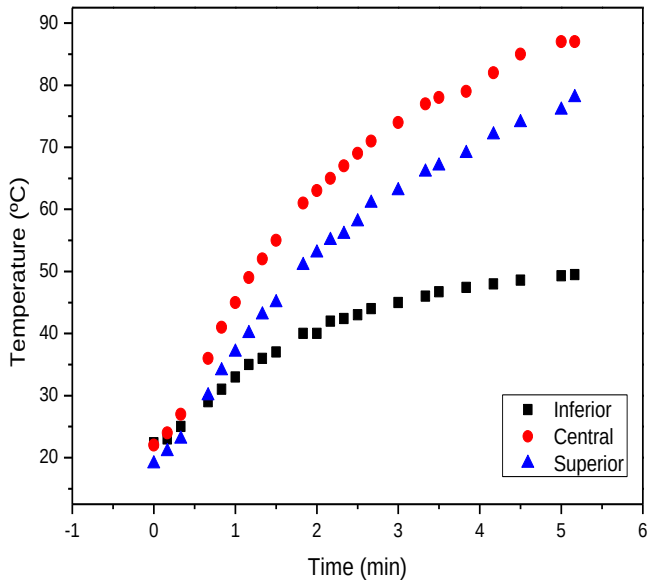

Fig. 3.12 a) PC temperature as function of sample position on the substrate holder for a current of 8,5 A.

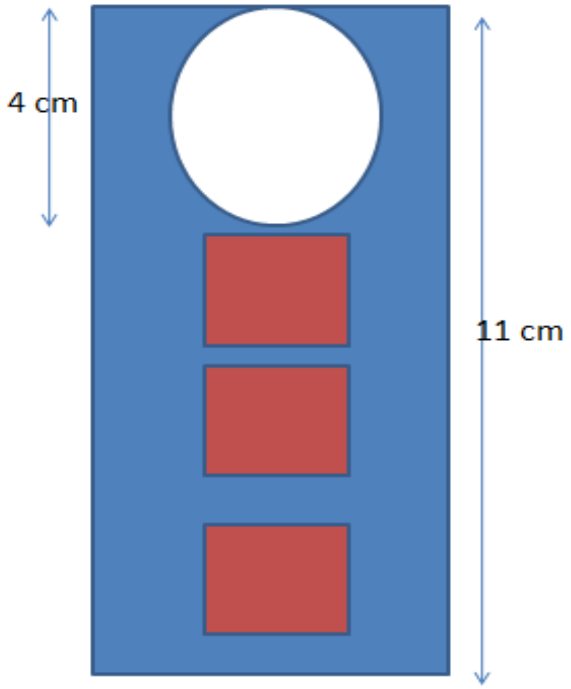

Fig. 3.12 b) PC samples assembly scheme correspondent to the previous figure.

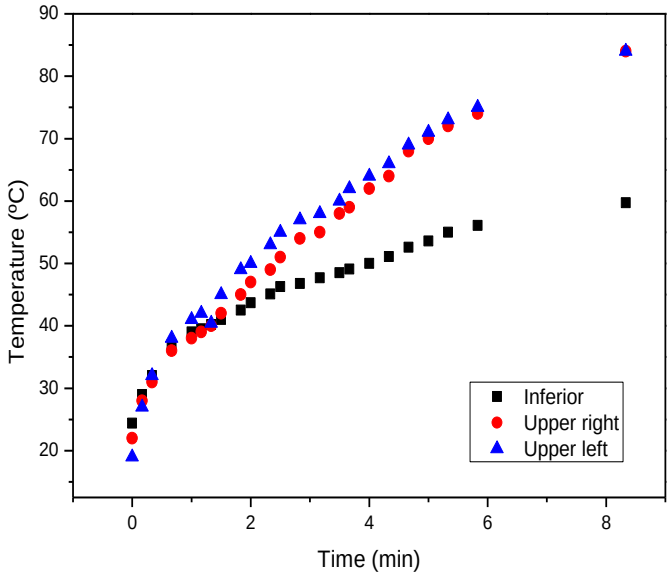

Fig. 3.13 a) PC temperature as function of sample position on the substrate holder for a current of approximately 9 A.

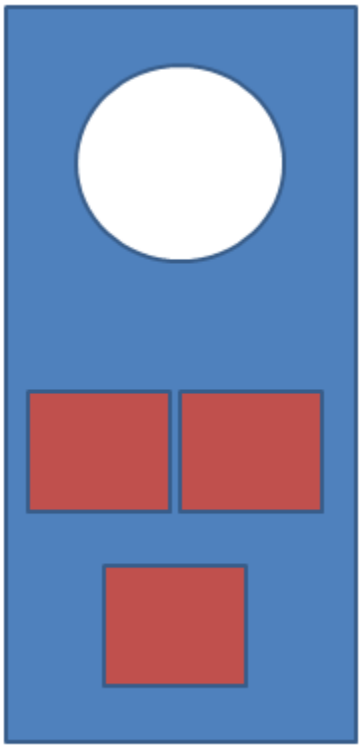

Fig. 3.13 b) PC samples assembly scheme correspondent to the previous figure.

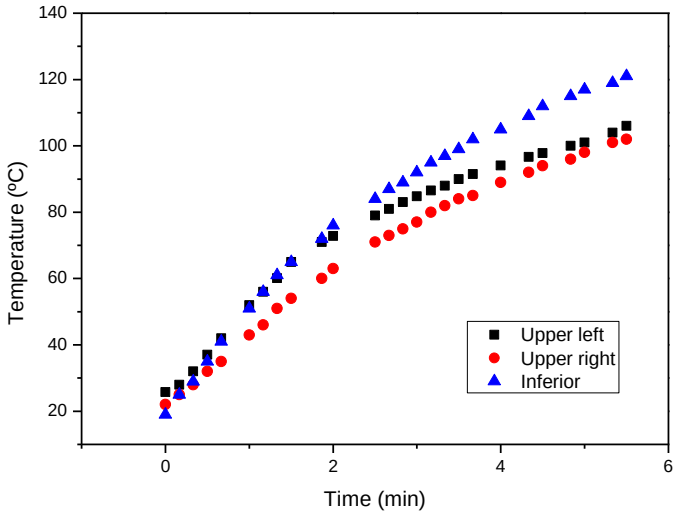

Fig. 3.14 a) PC temperature as function of sample position on the substrate holder for a current of approximately 11 A.

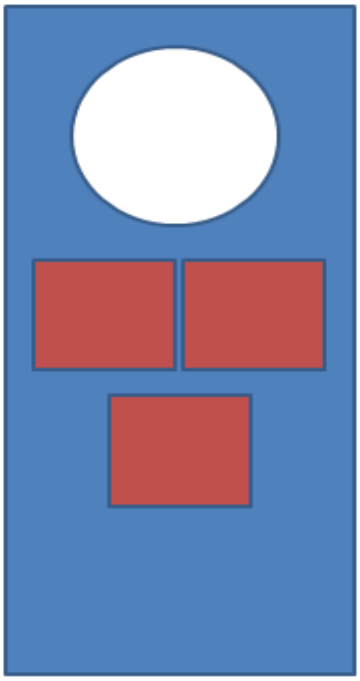

Fig. 3.14 b) PC samples assembly scheme correspondent to the previous figure.

From the data obtained with this study a working zone could be defined. Indeed, the sample placement displayed on fig. 3.14 b) seemed to be the most appropriate. However, regarding to the current applied on the Kauffman ion gun, none of the above referred currents could be employed. Indeed, with the elapse of experiments, a difficulty in controlling the ion gun for these lower currents was verified, with this source's often switch offs. Thus, it was operated on the lower current possible to be monitor (I = 13A).

Fig. 3.15 shows a real assembly of the samples considered in fig. 3.14 b) with the Kauffman ion gun switch on. Indeed, from the picture, one can claim a higher ion beam uniformity within the considered working zone compared with the entire substrate holder area. This substrate assembly was used for all the further experiments with polycarbonate.

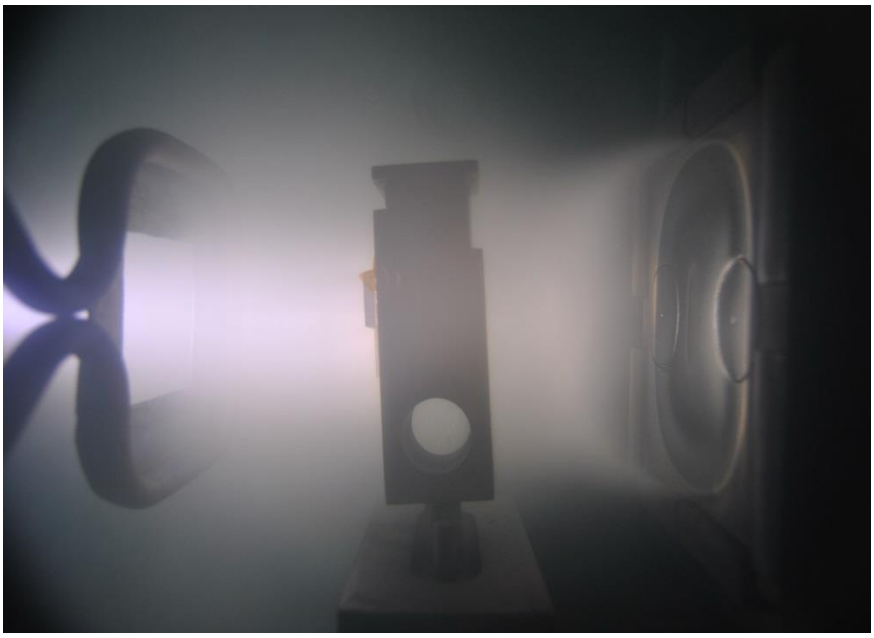

Fig. 3.15 – Polycarbonate substrates assembly

3.3.2 Plasma etching effects

In this sub-chapter, the effect of etching plasma treatment using an inert gas (argon) was studied. Three different etching treatments were applied, consisting on the same conditions except time, which was set at 1, 2 and 4 minutes (3.3.2.1).

Since polycarbonate, as other thermoplastics, presents a chemical inert surface with an associated low surface energy [69] plasma treatment had to be used to activate its surface [70]. Plasma treatment removes loosely bonded impurities [69] and modifies the polymer's surface chemistry [71], creating new functional reactive and cross linking groups [69].

When a polymer suffers a plasma gas discharge, a surface bond breaking occurs, with the consequent creation of free-radicals [55, 71]. If the plasma treatment is made using an inert gas (Ar ou He), as there are no free-radical scavengers, the free radical may form a bond with another nearby free radical or with a radical in a different chain (crosslink) [71]; as well as it may rest as free radical, without any bonding [55].

Activation is more likely to occur when reactive gases are used for the plasma treatment, and consists on the replacement of surface polymer functional groups by different atoms or chemical groups present in the plasma [71].

Along with the surface chemical modifications, etching also promotes a more "grosser" effect on a polymer. Due to the ionic bombardment of the gas species, etching promotes a surface topographic change in the polymers, leading to a modification of its roughness [58].

3.3.2.1 Temperature variation of PC substrates during etching

Polycarbonate maximum temperature without damage is around 120 ˚ C [50]. So, the maximum time of exposure which would bring the PC to that temperature was measured (4 minutes), and two more inferior times of treatment were defined (1 and 2 min). The temperature was measured for the three etching treatment times.

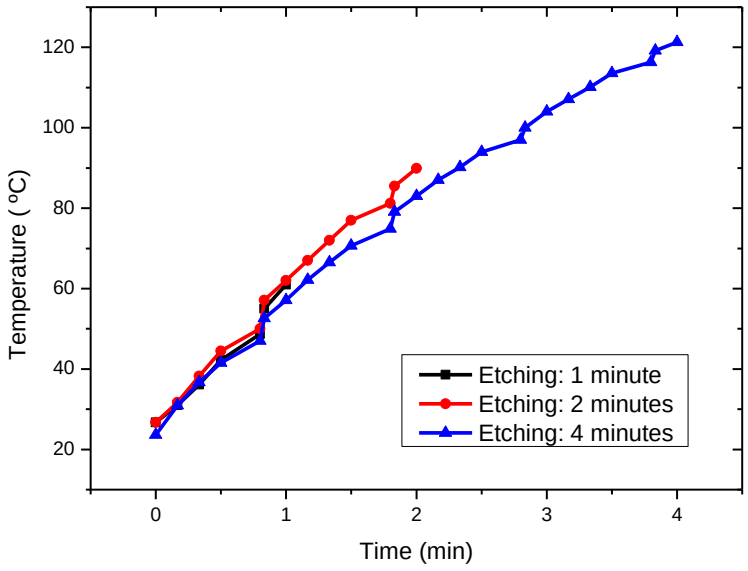

Fig. 3.16 – PC temperature variation for three different etching treatments.

From the curve analysis in any of the three variations shown above (fig 3.16), one may observe some curve discontinuities, which are related to the difficulties in controlling

the ion gun, which was set at I = 13A. The defined current was difficult to monitor, and likely to decrease during treatment so that it needed to be continuously controlled. Occasionally it turned off, being quickly switch on again. In that case, the switch on of the source led the current to a spike that also disturbed the experiment. These anomalies inflicted a higher temperature increase when compared with the smooth increase provided by the fixed 13 Amperes.

3.3.2.2 Roughness

The average roughness values were obtained recurring to Atomic Force Microscopy.

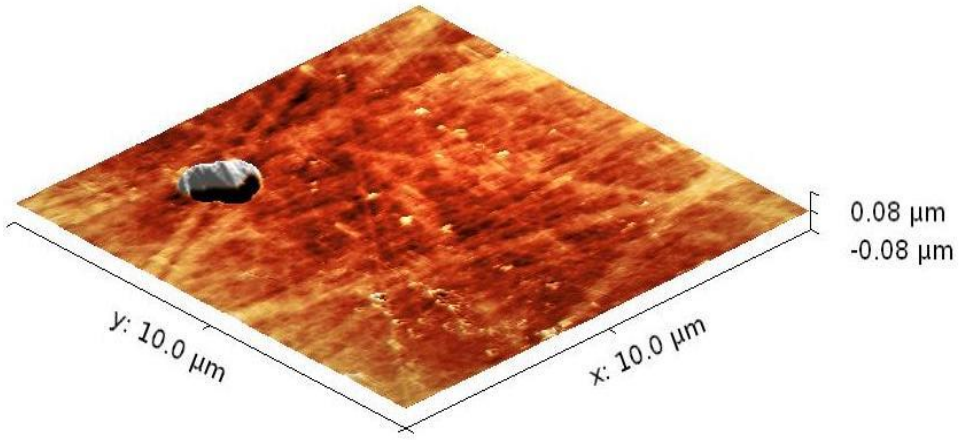

Fig 3.17 a) - Topographic view of an untreated PC sample

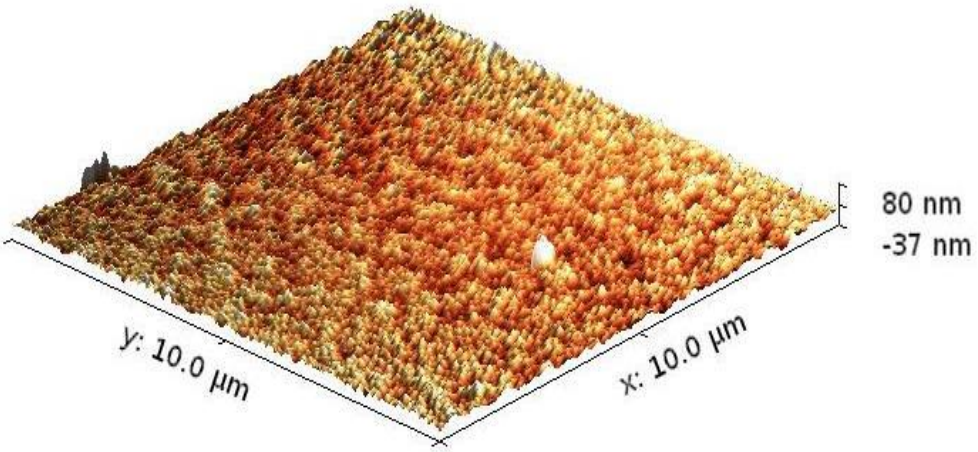

Fig 3.17 b) – Topographic view of a PC sample with 4 minutes etching treatment

Fig 3.17 shows the surface modification of polycarbonate due to etching treatment. It is possible to notice a clear topographic surface modification pattern, from the untreated sample to the sample with higher treatment time. On the presented topographic views there are some imperfections that do not represent the plasma treatment. These correspond to defects already present in the original surface (fig 3.17 a) and were not taken into account for the Ra calculation.

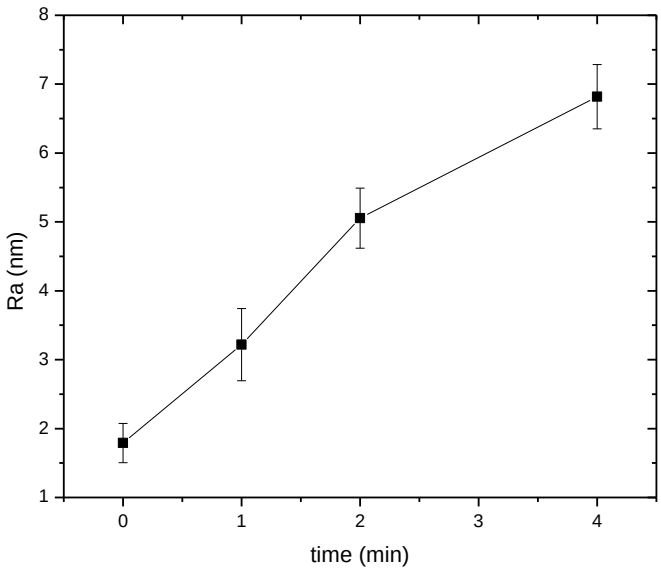

Fig 3.18 – The advancing Ra for different treatment times

The Ra obtained values (presented in fig 3.18), Ra(0)=1,79 nm; Ra(1)=3,218 nm; Ra(2)=5,054 nm and Ra(4)= 6,810 nm, confirmed a roughness increase with the increase of treatment time, as it was expected [55, 58, 72]. This roughness change happens due to a continuous removal of top atomic layers of polymer during etching [72], so it is correct to assume that for a higher treatment time, more removal occurs, with a consequent higher roughness achievement.

3.3.2.3 Wettability

For contact angle measurement the sessile drop method was used. The obtained values are presented on fig 3.19.

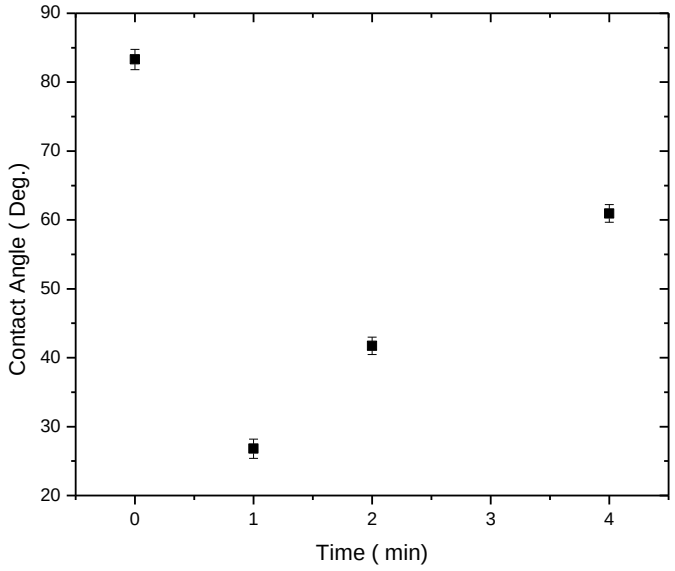

Fig 3.19 – Contact angle evolution for the different etching treatment times

From contact angle analysis (fig. 3.19) one can conclude that PC wettability was improved, as expected [55, 70, 72]. Indeed, the contact angle for each of the three treatments was inferior to the CA calculated for the untreated PC (C.A.(0) = 83˚; C.A.(1) = 27 ˚; C.A.(2) = 42 ˚; C.A.(4) = 61 ˚).

Regarding the overall C.A. evolution in comparison with the observed roughness increase (fig 3.18), a C.A. decrease was expected since, from Wenzel's equation, a hydrophilic surface (C.A < 90º) becomes rather hydrophilic under a roughness increase [58, 72]. The observed contact angle increase from the 1 minute treatment to higher time treatments leads, thus, to the conclusion that the influence of roughness can be ruled out, and the contact angle evolution can only be explained in terms of chemical surface changes.

For the 1 minute treatment time, the rather small CA value obtained (27 º) can be a consequence of the plasma damage of the surface associated with the post-plasma oxidation of the formed radicals. Upon atmospheric exposure, the formed free-radicals can react with oxygen forming polar oxygenated groups, giving rise to a highly hydrophilic surface [55] which is more likely to display a higher affinity with water, thus, when a water drop is syringed onto a surface with these characteristics a high water dispersion may be observed.

Regarding the C.A. evolution throughout the higher treatment times, a decrease of contact angle was expected, as a response to a more hydrophilic behavior [55, 72] derived from a major polar group creation with more exposure to etching [72]. However, as opposed, a contact angle increase was verified.

This unexpected C.A. increase can be a consequence of the cross linking effects which occur during etching. One may assume that with the increase in treatment time, there is an increase in the concentration of free-radicals formed, and it is more likely to occur cross linking than for the 1 minute treatment time. This was not observed in other studies with polycarbonate [70, 72, 69]; however none of these studies used an ion gun for the etching of this polymer, and thus the plasma conditions were different.

Another explanation for the contact angle increase verified from the 1 minute treatment to the 2 and 4 minutes treatment may arise from the used etching system:

When a Kauffman ion gun is used for the cleaning of a surface, a contamination provided by a parasitic ion implantation can occur [73]. On the other hand, the water contact angle in a polycarbonate surface was already found to increase as a consequence of the implanted energy due to ion implantation on its surface. A higher ion implementation is translated into a higher implanted energy and a consequent higher value of contact angle is obtained [74].

It is possible to assume that a parasitic ion implantation occurred on PC surface during the plasma treatments, and that this ion implantation was growing as the treatment time increased (notice, from fig 3.16, that the temperature attained on polymer's surface for the 4 minutes plasma treatment was approximately the double of the one attained with 1 minute of treatment). Hence, the treatments with 2 and 4 minutes may comprise an implanted energy high enough to interfere with the water drop dispersion, contrary to what was observed for the 1 minute treatment time.

The explanation for the contact angle evolution could only be confirmed by employing more sophisticated surface analysis techniques such as XPS to analyze chemical bonding or Raman and/or IR to analyze molecular structures.

3.3.3 AlN_x thin film deposition onto PC substrate

3.3.3.1 PC temperature evolution during the deposition process

Fig. 3.20 shows the Polycarbonate temperature evolution during the entire deposition process.

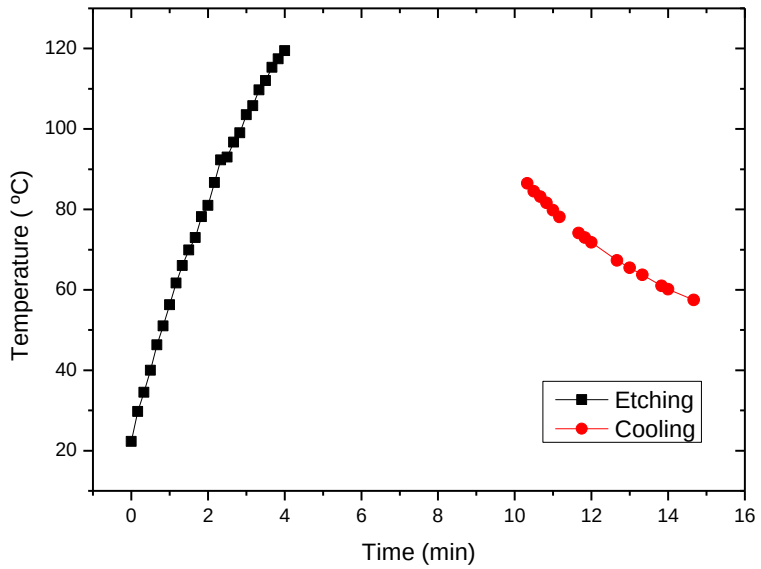

Fig. 3.20 – PC temperature evolution during the deposition process, for an etching treatment of 4 minutes.

Fig. 3.20 shows the polycarbonate temperature evolution for the longer etching treatment time. At the end of the etching treatment, a temperature of 119ºC was achieved on polycarbonate. After the etching treatment, the target power supply was switch on and a delay time of 3 minutes was taken before placing the substrate in front of the target, in order to allow its surface cleaning. Thus, and given the thermocouple limitations, the temperature was measured again only in the end of the deposition, in which the polycarbonate sample was at 86,5º C.

3.3.3.2 Adhesion

The X – cut test was used, according to the ASTM standard D 3359-08, in order to verify the effects of the different plasma treatment times in films adhesion.

The presented adhesion results correspond to films deposited with the same nitrogen partial pressure ratio (0,133). Figures 3.21, 3.22 and 3.23 show the surface aspect (obtained with optical microscopy) of the coated PC samples prior to the application of the sensitive tape and after its removal.

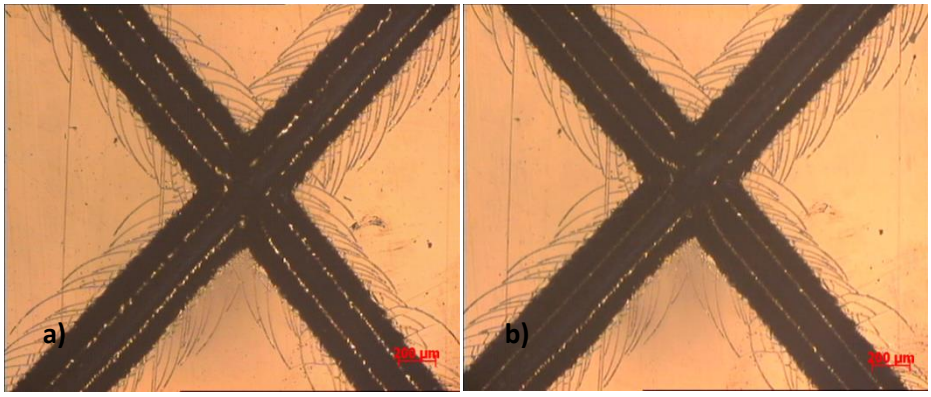

Fig 3.21 Coated PC with 1 minute of plasma treatment: a) prior and b) after de tape removal.

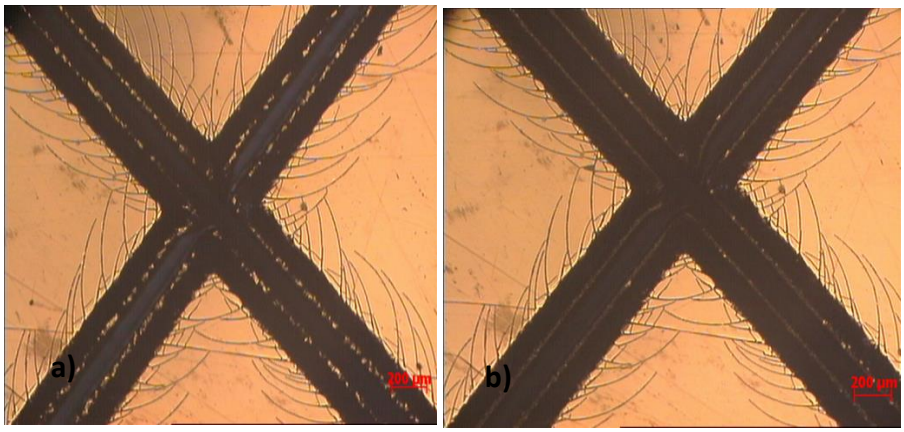

Fig 3.22 Coated PC with 2 minutes of plasma treatment: a) prior and b) after de tape removal.

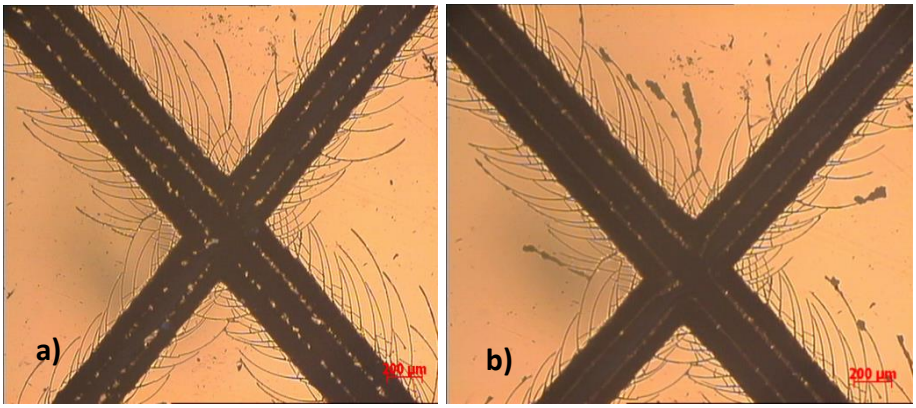

Fig 3.23 Coated PC with 2 minutes of plasma treatment: a) prior and b) after de tape removal.

All the coatings presented a quite good adhesion, although minor delamination can be observed in the 4 minutes etching coating (fig. 3.23 b)). Indeed, the 1 and 2 minutes of plasma treatment coatings displayed no signs of film delamination upon the pressure sensitive tape removal; thus, according to the ASTM standard D 3359-08, they can be classified as 5A (no peeling or removal), while the 4 minutes of etching coating can be rated as 4A (Trace peeling or removal along incisions or at their intersection).These observations confirmed the obtained data from contact angle evaluation. Thus, the 4 minute plasma treatment can, in fact, be considered as the less well succeeded treatment.

The observed cracks along the incisions (in any of the coatings) are a consequence of the stress induced during the cut, and the differences in the amount of cracks are possibly dependent on the pressure exerted on the cut tool.

The fact that no significant adhesion difference was observed between the first two etching treatments may be due to the deposition conditions. Indeed, the higher the kinetic energy of the incident species, the better the film's adhesion is [36]. Thus, the previously referred deposition conditions were, possibly, enough to promote the same adhesion on polycarbonate substrates with two different surface energies, and from this assumption both the etching treatments can be considered equally efficient for the AlN_x thin film deposition under the presented conditions.

3.3.3.3 Morphology

Films´ morphology was assessed using Scanning Electron Microscopy. AlN_x films, due to their lower conductivity, were recoated with a 20-30 nm layer of gold.

Fig 3.24 shows cross sections of an AlN_x film deposited onto a polycarbonate substrate.

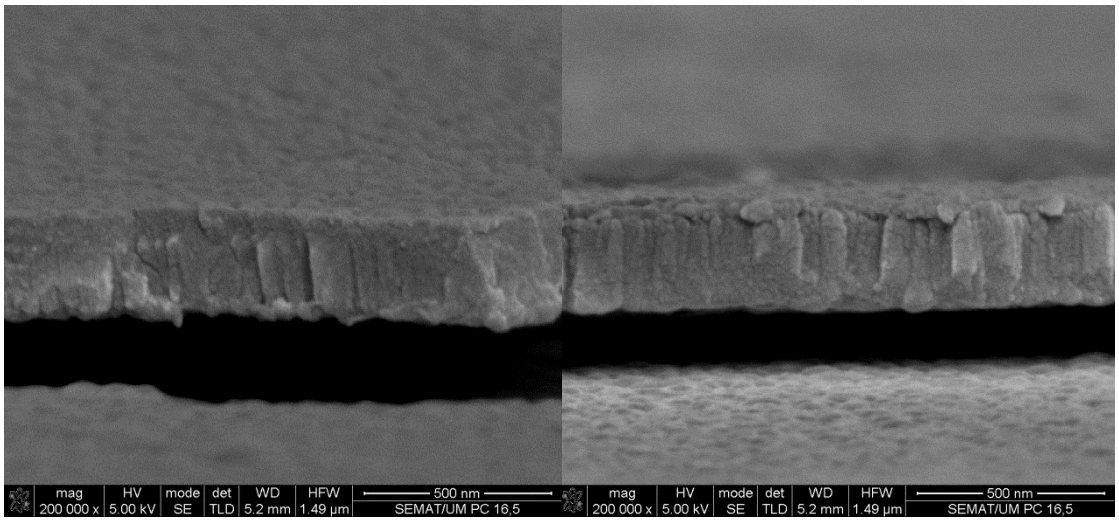

Fig 3.24 Cross sections and of a AlN_x thin film deposited with P_{N2}/P_{Ar} = 0,140 onto a PC substrate

From fig. 3.24 analysis, it is possible to notice a non-pronounced columnar structure is possible. Indeed, a disordered morphology is observed, with zones with a characteristic columnar growth, and feature-less dense zones, without any order of arrangement. From the film top view, although not well focused, it is possible to observe the same granular surface visible for the AlN_x films deposited onto glass. Thus, one may assume that under these deposition conditions the AlN_x thin film grows with a randomly mesh structure from columnar to dense.

This observed morphology is consistent with the amorphous structure observed for the X-Ray diffraction studies in which this nitrogen partial pressure was considered. Nevertheless, even if the deposition conditions (high deposition power in a static mode) were previously considered to be responsible for a tendency for crystallization of an expected totally amorphous structure, on the other hand the lower temperatures associated to the film deposition (fig. 3.20) have to be considered regarding its implications on low surface mobility of the condensing species, and consequent structure's Amorphization [66]. Thus, both effects must be considered and assumed to be the cause of this non-pronounced columnar growth.

3.3.3.4 Resistivity

The resistivity of the AlN_x thin films deposited onto polycarbonate was measured using the four probe method at RT. However, film's thicknesses could not be evaluated. Thus, for the presented values, a thickness of 250 nm was considered for all the measured film. This approximation was deemed acceptable given the lack of accuracy when measuring such thinner films using profilometry. Table 3.2 contains the obtained values for AlN_x films' resistivity.

Table 3.2 – Film's resistivities measured for AlN_x films deposited onto polycarbonate.

Nitrogen partial pressure ratio	Resistivity (Ohm.cm)
	$\rho = 2{,}3 \times 10^{-2}$
$P_{N2}/P_{Ar} = 0{,}133$	$\rho = 1{,}3 \times 10^{-2}$
	$\rho = 1{,}8 \times 10^{-2}$
$P_{N2}/P_{Ar} = 0{,}140$	$\rho = 1{,}1 \times 10^{-2}$
	$\rho = 2{,}1 \times 10^{-2}$

From the obtained values (table 3.2) it is possible to observe an overlap of resistivities for the two different nitrogen partial pressure ratios, which is coherent with the obtained data from film's chemical compositions. Due to the inexistence of films correspondent to the nitrogen partial pressure ratio of 0,147 when this measurement took place, no reference is made to these films in the table.

However, these values are extremely important for this thesis purpose, since they justify an integral AlN_x thin film growing onto the polycarbonate substrate. Furthermore, despite the fluctuations, they are coherent with the obtained resistivities for films deposited onto glass, and are within the intended resistivity range.

Chapter 4
Conclusions

This thesis had the purpose to deposit a 200-300nm AlNx thin film onto a suitable polymeric basis, within a desired film electrical resistivity (from 1x10-3 to 1x10-1 ohm.cm), using as magnetron sputtering the deposition technique.

After a first approach in which film's hardness and resistivity were assessed using silicon and glass as substrates, the nitrogen partial pressure ratio range appropriate to serve this goal was determined. The effect of nitrogen content increase in film's resistivity was verified.

Within this range a more detailed study was carried, in terms of studying chemical composition, structure and morphology evaluations. Films revealed to be amorphous (with broad peaks possibly precursors of the (002) orientation of the stoichiometric aluminium nitride), to growth in a non-well defined columnar structure and, more important, revealed that within such a small range of nitrogen partial pressure ratios, its nitrogen content can be overlapped.

Serving the purpose of the project, the AlNx films were deposited onto polymers. Polyurethane was the first choice to act as substrate, however it revealed to be unsuitable given its curvature under heat; thus the deposited AlNx films revealed cracks on their structure due to their lower elasticity compared to a polymer. Polycarbonate, on the other hand, seemed to serve as substrate. Indeed, from the first depositions no crack formation was verified on films' structure.

To better study the AlNx deposition onto polycarbonate, three different etching conditions (3 different treatment times) were applied to this substrate. The results showed that two of these treatments (the one and two minutes treatment) promoted a very good adhesion of the AlNx films.

The resistivity of AlNx films deposited onto the polycarbonate substrate was evaluated, and although the impossibility of accurate resistivity measurement, these results were extremely important since they pointed out the same resistivity achievement of the films deposited onto glass, what may be related with the same film growth in both substrates. Moreover, these data allowed concluding the AlNx films integrity when deposited onto polycarbonate.

Finally, it can be concluded that conditions for the obtaining of films with the intended characteristics were defined, and can be reproducible.

References

[1] “Biopotential Electrodes” Avaliable at http://www.fis.uc.pt/data/20062007/apontamentos/apnt_134_5.pdf, accessed on 28/08/2013.

[2] Singh, Y.N., Singh, S.K., Ray, A.K., *Bioelectrical Signals as Emerging Biometrics: Issues and Challenges*. ISRN Signal Processing, 2012: 712032 (2012).

[3] Bronzino, J.D., *The biomedical engineering handbook: medical devices and systems*. 3rd ed. Taylor&Francis (2006).

[4] Chi, Y.M., Jung, T-P., Cauwenberghs, G., *Dry-Contact and Noncontact Biopotential Electrodes: Methodological Review*. Ieee Reviews In Biomedical Engineering, 3 (2010).

[5] Martins, A., *Desenvolvimento de biossensores não invasivos para captação de sinais eletroencefálicos baseados em alginato, com potencial utilização em recém-nascidos*. Master Thesis, University of Coimbra (2012)

[6] Action potential, Avaliable at http://psychlopedia.wikispaces.com/action+potential. Accessed on 01/09/2013.

[7] ECG / EEG Encyclopædia Britannica, *Action potential*, Available at http://www.britannica.com/EBchecked/topic/4491/action-potential. Accessed on 15/08/2013.

[8] Lee,T., Niederer P., *Basic Engineering for Medics and Biologists*, IOS Press, 2010.

[9] Brown, Z. Gupta, B., *Biological signals and their measurement*. Update in Anaesthesia: 164-169.

[10] Typical ECG tracing of the cardiac cycle.
Available at http://cardiac.northbayhealthcarenursing.com/ecg-waveforms.html. Accessed on 08/09/2013.

[11] Typical EEG waves.
Available at http://www.peakmind.dk/what_is_eeg.html. Accessed on 08/09/2013.

[12] Grozea, C., Voinescu, C.D., Fazli, S., *Bristle-sensors – Low-cost flexible passive dry EEG electrodes for neurofeedback and BCI applications*. Available at http://eprints.pascal-network.org/archive/00009479/01/bristle_sensors_JNE2011_preprint.pdf. Accessed on 25/05/2013.

[13] Invasive electrodes.
http://img.medscape.com/fullsize/migrated/560/817/ncpn560817.fig1.gif. Accessed on 26/08/2013.

[14] Zander, T.O., Lehne, M., Ihme, K., Jatzev, S., Correia, J., Kothe, C., Picht, B., Nijboer, F., *A dry EEG-system for scientific research and brain–computer interfaces*. Frontiers in Neuroscience, 5(53): 1-10 (2011).

[15] Fiedler, P., Pedrosa, P., Griebel, S., Fonseca, C., Vaz, F., Zanow, F., Haueisen, J., *Novel Flexible Dry PU/TiN-Multipin Electrodes: First Application in EEG Measurements*. 33rd Annual International Conference of the IEEE EMBS Boston, Massachusetts USA, August 30 - September 3 (2011).

[16] Sullivan, T.J., Deiss, S.R., *A brain-machine interface using dry-contact, low-noise EEG sensors*. IEEE International Symposium on Circuits and Systems, 2008. Available at http://www.isn.ucsd.edu/pubs/iscas08_eeg.pdf. Accessed on 29/05/2013.

[17] Salvo, P., Raedt, R., Carrette, E., Schaubroeck, D., Vanfleteren, J., Cardon, L. *A 3D printed dry electrode for ECG/EEG recording*. Sensors and Actuators A, 174: 96-102 (2012).

[18] Wet electrodes. Avaliable at http://medifactory.nl/images/foto/eeg/foto01.jpg Accessed on 01/09/2013.

[19] Gargiulo, G., Calvo, R.A., Bifulco, P., Cesarelli, M., Jin, C., Mohamed, A., van Schaik, A., *A new EEG recording system for passive dry electrodes*. Clinical Neurophysiology, 121: 686–693 (2010).

[20] Saab, J., Battes, B., Grosse-Wentrup, M., *Simultaneous EEG Recordings with Dry and Wet Electrodes in Motor-Imagery*. Available at http://mlin.kyb.tuebingen.mpg.de/BCI2011JS.pdf. Accessed on 25/05/2013.

[21] Ortner, R., Grünbacher, E., Guger, C., *State of the art in sensors, signals and signal processing*. Available at http://www.gtec.at/content/download/1659/10347/version. Accessed on 20/05/2013.

[22] Active dry electrodes. Available at http://www.cortechsolutions.com/Products/EC/EC-AC/EC-AC-DR. Accessed on 01/09/2013.

[23] Yang, Q., Cordery, S., Guy, R.H., *Application of Biophysics and Bioengineering to the Assessment of Skin Barrier Function*. Available at http://www.skin-forum.eu/posters/2010/quans_poster.pdf. Accessed on 23/05/2013.

[24] Eppstein, J., McRae, S., Papp, J. 2006, *Transdermal drug delivery device, method of making same and method of using same*, US Patent 7141034.

[25] Farris, P.K., *Skin Anatomy and Physiology*. Available at http://www.nuskin.com/en_ZA/corporate/company/science/skin_care_science/skin_anatomy_andphysiology.html. Accessed on 20/05/2013.

[26] Petersen, K.K., Rousing, M.L., Jensen, C., Arendt-Nielsen, L., Gazerani, P., *Effect of local controlled heat on transdermal delivery of nicotine*. International Journal of Physiology, Pathophysiology & Pharmacology, 30;3(3): 236-42 (2011).

[27] Park, J.-H., Lee, J.-W., Kim, Y.-C., Prausnitz, M.R., *The effect of heat on skin permeability*,International Journal of Pharmaceutics, 359: 94–103 (2008).

[28] Sexton, F.A., Rumson, N.J. 2010, *Transdermal device having mechanical assist for porator-to-skin contact*, US Patent 7853320 B1.

[29] Jadoul, A., Bouwstra J., Preat, V., *Effects of iontophoresis and electroporation on the stratum corneum. Review of the biophysical studies*. Advanced Drug Delivery Reviews, 35: 89–105 (1999).

[30] Eppestein, J., Hatch, M., Yang, D., Microporation of human skin for monitoring the concentration of an analyte, US Patent 5885211 A.

[31] Laser microporation of the skin: prospects for painless application of protective and therapeutic vaccines. Avaliable at http://www.ncbi.nlm.nih.gov/pmc/articles/PMC3667678/. Accessed 28/08/2013.

[32] Murthy, S.N., Sen, A., Zhao, Y.-L., Hui, S.W., *Temperature Influences the Postelectroporation Permeability State of the Skin*. Journal of Pharmaceutical Sciences, 93(4): 908-915 (2004).

[33] Oliveira, J., *Luminescência em revestimentos duros do sistema Al-N por dopagem com érbio*. Doctoral Thesis, University of Coimbra (2003).

[34] Vacandio, F., Massiani, Y., Gergaud, P. Thomas, O.*; Stress, porosity measurements and corrosion behaviour of AlN films deposited on steel substrates*. Thin Solid Films, 359: 221-227 (2000).

[35] Borges, J., Martin, N., Barradas, N., Alves, E., Eyidi, D., Beaufort, M., Riviere, J., Vaz, F., Marques, L.; *Electrical properties of AlNxOy thin films prepared by reactive magnetron sputtering*. Thin Solid Films, 520: 6709–6717 (2012).

[36] Wasa, K., Hayakawa, S. *Handbook of Sputter Deposition Technology: Principles, Technology and Applications (Materials Science and Process Technology Series)*.

[37] Anders, A.; *Plasma and ion sources in large area coating: A review*; Surface and Coatings Technology Volume 200, Issues 5–6**.**

[38] Kauffman ion Source. Available at http://www.ionbeam.co.uk/kaufmanionsource.asp. Accessed on 27/07/2013 .

[39] Donkov, N., Dinkov, Z., Ivanov, K.; *Ion source with hot filament and magnetic field. Model-based anode current control*. Vacuum, 69: 445–447 (2003).

[40] Mattox, D.M. *Handbook of Physical Vapor Deposition (PVD) Processing: Film Formation, Adhesion, Surface Preparation and Contamination Control*. Noyes Publications (1998).

[41] Kelly, P.J., Arnell, R.D., *Magnetron sputtering: a review of recent developments and applications*. Vacuum, 56: 159-172 (2000).

[42] Silva, A., *Optimização da deposição de filmes de hidroxiapatite para revestimentos de substratos de titânio poroso*. Master Thesis, Universidade de Coimbra (2012).

[43] Fonseca, P., *Filmes finos para sensores de pressão em próteses de membros inferiores: dióxido de titânio dopado com prata*. Master Thesis, Universidade de Coimbra (2011).

[44] Cavaleiro, A., Vieira, M.T, Textos de apoio às disciplinas de Engenharia de Superfícies e degradação e protecção de superfícies (1995).

[45] Parreira, N., *Synthesis and characterization of reactive magnetron sputtered W-O-N coatings*. Doctoral Thesis, University of Coimbra (2008).

[46] Cunha, L., *Desenvolvimento de eléctrodos secos para electroencefalografia*, Universidade do Porto (2008).

[47] Carter, D., *Arc reduction in magnetron sputtering of metallic materials*. Advanced Energy Industries, Inc. Available at http://www.advanced-energy.com/upload/File/White_Papers/ENG-ArcSputmetal-270-01.pdf. Accessed on 27/07/2013

[48] Kelly, P.J., Bradley, J.W., *Pulsed magnetron sputtering – process overview and application*. Journal of optoelectronics and advanced materials, 11(9): 1101 – 1107 (2009).

[49] Biresin® U1419 Technical Data Sheet. Available at http://toolingandcomposites.sika.com/. Accessed on 30/08/2013.

[50] Tecanat datasheet. Available at http://www.sdplastics.com/ensinger/TECANAT.pdf. Accessed on 30/08/2013.

[51] Pappas, D., Copeland, C., Jensen, R.; *Wettability Tests of Polymer Films and Fabrics and Determination of Their Surface Energy by Contact-Angle Methods*; available at http://www.dtic.mil/dtic/tr/fulltext/u2/a466437.pdf. Accessed on 04/07/2013.

[52] Escudeiro, A., *Estudo do comportamento tribológico em ambientes biológicos de revestimentos DLC dopados com Ti*. Master Thesis, Universidade de Coimbra (2010).

[53] Stalder, A. *Drop shape analysis*. Available at http://bigwww.epfl.ch/demo/dropanalysis/. Accessed on 28/07/2013.

[54] *Information on contact angle*. Available at http://www.ramehart.com/contactangle.htm. Accessed on 28/07/2013.

[55] Lima, P., Pedrosa, P., Machado, A., Fonseca, C., Vaz, F.; *Plasma Surface Activation and TiN Coating of a TPV Substrate for Biomedical Applications*. Plasma Processes and Polymers, 8: 1174–1183 (2011).

[56] Stalder, A.F., Kulik, G., Sage, D., Barbieri, L., Hoffmann, P., *A snake-based approach to accurate determination of both contact points and contact angles*. Colloids and Surfaces A: Physicochemical And Engineering Aspects, 286(1-3): 92-103 (2006).

[57] Schweitzer, J., *Scanning Electron Microscope*. Available at http://www.purdue.edu/rem/rs/sem.htm. Accessed on 30/08/13.

[58] Pedrosa, P., Chappé, J.-M., Fonseca, C., Machado, A.V., Nóbrega, J.M., Vaz, F., *Plasma Surface Modification of Polycarbonate and Poly(propylene) Substrates for Biomedical Electrodes*. Plasma Processes and Polymers, 7(8): 676–686 (2010).

[59] Gutiérrez, M.P., Li, H., Patton, J., *Thin Film Surface Resistivity*, San José State University (2002) Available at http://www.sjsu.edu/faculty/selvaduray/page/papers/mate210/thinfilm.pdf. Accessed on 28/07/2013.

[60] Gomes, L., *Desenvolvimento de novos biossensores para eletroencefalografia baseados em poliuretano revestido com tiagx*, Master Thesis, Universidade de Coimbra (2012).

[61] Borges, J., Martin, N., Barradas, N.P., Alves, E., Eyidi, D., Beaufort, M.F., Riviere, J. P., Vaz, F., Marques, L., *Electrical properties of AlNxOy thin films prepared by reactive magnetron sputtering*. Thin Solid Films, 520(21): 6709–6717 (2012).

[62] Borges, J., Vaz, F., Marques, L., *AlNxOy thin films deposited by DC reactive magnetron sputtering*. Applied Surface Science, 257(5): 1478–1483 (2010).

[63] Vaz, F., Ferreira, J., Ribeiro, E., Rebouta, L., Lanceros-Méndez, S., Mendes, J.A., Alves, E., Goudeau, P., Rivière, J.P., Ribeiro, F., Moutinho, I., Pischow, K., de Rijk, J., *Influence of nitrogen content on the structural, mechanical and electrical properties of TiN thin films.* Surface & Coatings Technology, 191: 317–323 (2005).

[64] Polcar, T., Parreira, N.M.G., Cavaleiro, A., *Tribological characterization of tungsten nitride coatings deposited by reactive magnetron sputtering*. Wear, 262: 655-665.

[65] Borges, J., Barradas, N. P., Alves, E., Beaufort, M.F., Eyidi, D., Vaz, F., Marques, L., *Influence of stoichiometry and structure on the optical properties of AlNxOy films*. Journal of Physics D: Applied Physics, 46(1) (2013).

[66] Jin, H., Zhou, J., Dong, S.R., Feng, B., Luo, J.K., Wang, D.M., Milne, W.I., Yang, C.Y., *Deposition of c-axis orientation aluminum nitride films on flexible polymer substrates by reactive direct-current magnetron sputtering*. Thin Solid Films, 520: 4863–4870 (2012).

[67] Pei, Y.T., Bui, X.L., van der Pal, J.P., Martinez-Martinez, D., Zhou, X.B., De Hosson, J.Th.M., *Flexible diamond-like carbon films on rubber: on the origin of self-acting segmentation and film flexibility*. Acta Materialia, 60: 5526–5535 (2012).

[68] Hutchinson, J.W., *Stresses and failure modes in thin films and multilayers: notes for a dcamm course*. Technical University of Denmark (1996).

[69] Subedi, D. P., Madhup, D. K., Adhikari, K., Joshi, U. M., *Plasma treatment at low pressure for the enhancement of wettability of polycarbonate*. Indian Journal of Pure & Applied Physics, 46(08): 540-544 (2008).

[70] Chena, T.N., Wuua, D.S., Wua, C.C., Chianga, C.C., Lina, H.B., Chena, Y.P., Horngb, R.H., *Effects of plasma pretreatment on silicon nitride barrier films on polycarbonate substrates*. Thin Solid Films, 514: 188–192 (2006).

[71] Wolf, R., Sparavigna, A.C., *Role of Plasma Surface Treatments on Wetting and Adhesion*. Engineering, 2: 397-402 (2010).

[72] Vijayalakshmi, K. A., Mekala, M., Yoganand, C. P., Navaneetha Pandiyaraj, K., *Studies on adhesive properties of polypropylene (PP) and polycarbonate (PC) film surfaces using DC glow discharge plasma*. International Journal of Physical Sciences, 7(15): 2264-2273 (2012).

[73] von Bohlen, A., Klockenkämper, R., *Parasitic ion-implantation produced by a Kaufman-type ion source used for planar etching of surfaces*. Analytical and Bioanalytical Chemistry, 382(8): 1975-80 (2005).

[74] - Lee, C.Y., Kil, J.K., *Hydrophilic property by contact angle change of ion implanted polycarbonate*. Review of Scientific Instruments, 79: 02C508 (2008).